Seismological Research Letters

NESS v1.0: A worldwide collection of strong-motion data to investigate near source effects

--Manuscript Draft--

Manuscript Number:	SRL-D-18-00149R1
Full Title:	NESS v1.0: A worldwide collection of strong-motion data to investigate near source effects
Article Type:	Article - Regular Section
Corresponding Author:	Francesca Pacor INGV MILAN, ITALY
Corresponding Author Secondary Information:	
Corresponding Author's Institution:	INGV
Corresponding Author's Secondary Institution:	
First Author:	Francesca Pacor
First Author Secondary Information:	
Order of Authors:	Francesca Pacor
	Chiara Felicetta
	Giovanni Lanzano
	Sara Sgobba
	Rodolfo Puglia
	Maria D'Amico
	Emiliano Russo
	Georgios Baltzopoulos
	Iunio Iervolino
Order of Authors Secondary Information:	
Manuscript Region of Origin:	ITALY
Suggested Reviewers:	
Opposed Reviewers:	

Associate Editor comment

0. SRL has "Data Mine" (https://www.seismosoc.org/publications/srl/srl-data-mine-author-information/). We are currently looking for manuscripts that provide databases of seismological parameters (e.g., relocation earthquake catalog, slow-slip earthquake database) for Data Mine. I feel that this manuscript would fit to Data Mine. Please consider submitting the revised manuscript in the Data Mine category.

We agree that our paper is mainly focused on the presentation of a dataset. However, the manuscript is significantly longer than 3000 words, which is the limit for Data Mine paper. In fact, it is more than a pure dataset description, since it is accompanied by several (preliminary) analyses that highlight significant features of near-source ground motions. Therefore, we prefer not to shorten to a Data Mine paper, so as not to cut material that we consider valuable research and that may be useful for others. Nevertheless, in order to reduce the length of the manuscript, we decided to move some figures in the Electronic Supplement, as also suggested

1. L195. high-pass frequencies <= 0.1 Hz

This may be "high-pass frequencies >= 0.1 Hz"?

Yes, we corrected the sentence.

2. Predictions (L254, L259).

There are several "predictions". I may have missed some information, but it is unclear how those predictions are computed? Please clarify this.

The predictions are the median values of the model proposed by Campbell and Bozorgnia (CB14, 2014). Now it is specified.

3. label "(a)", "(b)".

Several figures (Figs, 5,6,7,8,10,11,12,13,14,15,16) do no have "(a)", "(b)" labels (please see SRL Submission Guidelineshttps://www.seismosoc.org/publications/srl-authorsinfo/).

Done.

Additional comments from EIC:

1. You have several tables with very long columns. Please consider putting them in the electronic supp. material. See guideline at https://www.seismosoc.org/publications/esupps/

2. You have 16 figures, while SRL normally do not allow more than 10 figures. Please put some figures into electronic supp.

3. Please put the panel IDs to the top left or right (and inside each panel) to keep the figures tight.

We moved some Tables and Figures to the Electronic Supp. Now, the manuscript has 2 tables and 10 figures.

Reviewer #1

1. please review the grammar and the style of hyphenation; I spotted some mistakes and inconsistencies while reading and I encourage the authors to carry out a careful read through;

Done.

2. Page 3, line 50. The authors might want to add Faccioli et al., 2004 (http://earthquakespectra.org/doi/abs/10.1193/1.1707022).

Done.

3. Page 8, line 181. Citing (CEN, 2004) makes this passage a bit Eurocentric. Please add also the NEHRP classes to the flat-file tables.

Done.

4. Page 10, line 227. I am not sure "Mimic" is the right verb here.

We removed the sentence (see reply to reviewer 2).

5. Figure 6 and elsewhere. Exceptional or Extreme? Please homogenize terminology.

We used overall in the text the term "Exceptional".

6. Figure 5. The units in the titles of the PGV subplots are wrong.

Done. The Figure was moved in the Electronic Supp.

Reviewer #2

1) My only real concern is the magnitude-dependent distance cutoff on the dataset (Figure 3a). When this dataset is used for analysis, this could cause biases. I think this restriction is discussed in the introduction/first line to the (Strong Motion waveforms). First off, that discussion is a little unclear as to what you are doing. Please reword to make it more clear that you are coming up with a physical basis on which you'll put a maximum distance restriction for record selection. At line 136, be clear that k=1 indicates you're considering records only within 1 fault length. But secondly, when I look at the Figure 3, I am concerned that this restriction is too limiting for the smaller magnitude data. Yes, I understand you want to focus on near-fault effects, but that will be hard to do if you don't have a baseline for the slightly farther ground motions, especially to compare to other GMPEs/databases.

We are aware that the (arbitrary) choice of k=1 may reduce the number of selected data, especially if you want to calibrate a ground motion model. Indeed, when we consider k=2, the number of records increases to about 1500. Since the focus of our study is to provide a set of data with remarkable near source effects, we decided to adopt this limit. In any cases, this dataset can be profitably used as support for testing and validating existing GMPEs and calibrate near source correction terms. In a future releases, after the user's feedbacks, we can enlarge this dataset, modifying the selection criteria (i.e., larger k values and different stress drop values) and adding a flag to identify the records with clear near source effect (e.g. the pulse-like or exceptional records).

2) Use of "strong" to modify "motion": The phrase "strong motion" when referring to a data type or instrumentation really just means "accelerometer." The words "strong motion," in other contexts, however, actually imply that the recorded motion was "strong" (whatever threshold the reader interprets "strong" to mean). "Strong motion" instruments actually record motions that are not very strong. Therefore, I strongly encourage you to be very clear that you mean accelerometer data. (i.e., line 15, line 84 here even more important, since it is vague). And in many other places.
I suggest you consider "significant" which can capture most of the intended effects.

We thank the reviewer for the suggestion. We substituted the term "strong motion" with "accelerometric data" where necessary.

3) Introduction: In the introduction, you have a nice discussion of how GMPEs consider near-source ground motions. However, in that, you have no discussion of the finite-fault effect/near-source saturation term/pseudo-depth term (whatever you'd like to call it) which is introduced by GMPE modelers to account for saturation of motion near to a large fault. I think this would be worthy of discussion here. See Thompson and Baltay (2018) for more discussion of this effect.

We added a short discussion on this point in the introduction, following the suggestion of the reviewer.

At the end of the intro, (near lines 70-75), you give empty words that you will show “evidence of well recognized effects” and “scaling of such effects” is evaluated. It would be better to actually say what these preliminary observations are. As it stands, these sentences are “empty”, they do not give the reader any insight. Does your data support or not what you would expect to see in the near source region? Do you observe the polarized ground motions and hanging-wall effects? Just state what the general observations are rather than saying that you’re going to tell us!

We modified the sentences, summarizing some general observations.

4) Peak ground motion distributions. It’s great that there are some plots showing general trends of this database with mag, distance, etc, and I especially like the discussion of the extreme values. However, the discussion of some of these ground motion features is a little weak in several places, and I think the discussion makes some claims that the data doesn’t back up. I would suggest just cutting a few of those sentences, since your paper does not depend on these conclusions. Distance saturation: (Line 230ff): I don’t think this data can demonstrate this statement; I’d suggest you simply delete this sentence. Also I don’t think the sentences on line 235-238 is relevant to this discussion, you haven’t shown or discussed the data at longer periods… also the hinge magnitude isn’t the magnitude saturation, its simply a magnitude at which the slope changes to capture the rough features of the GMPE. Line 239-242: I don’t see how your observations support this statement, furthermore, the statement is fairly vague and unsubstantiated.

Following the reviewer’s suggestion, we remove some the comments of lines 230 and 235-238. The sentences relative to the possible causes of the generation of exceptional values were rephrased, citing previous studies on this topic, just to support our comments.

5) Reference to Ancheta et al., 2014. Many (most?) of your events are contained in the NGA-West2 database. How do your source, site, path/distances parameters compare to theirs?

39 events are common between the two databases. The 50% have different fault geometries, since they are inferred from others studies and regional databases. Comparing magnitude and fault dimensions (length and width), we found a good agreement in term of magnitude; on the contrary, fault lengths and widths can differ, especially for multi-segment rupture for which, we considered only the dominant fault segment.

The differences observed on fault dimension have obviously an impact on the rupture distances (Rrup): if the dimensions of the faults differ for 10%, the percent differences between the NESS-Rrup and NGA-West2-Rrup are below 20%.

6) Are these crustal or subduction events? Can you please be clear about this?

We selected only crustal events; we now stated it in the text.

7) Abstract: Please give the distance restrictions of the database.

Done.

8) Earthquakes: say briefly where in the world they are coming from. And I suggest (see below) that you add a map of this distribution, and reference it here.

We added a map, with the distribution of the selected events.

9) Stress drop: Although it doesn’t much mater here, 1 MPa (10bars) average stress drop is pretty low, I think? Especially for the events that you mention (Long Beach, New Zealand, Japan, Italy). For California and Japan, an average of 3MPa – 5MPa is better.

We agree with the reviewer, we adopted the lower bound of the stress-drop range to include a larger number of waveforms; indeed, as the stress drop increases, the near-source distance Rns diminishes, as reported in the following table.

M/Ds	100bar	10bar	1bar
M=5.5	6	15	30
M=6.5	20	50	100
M=7.5	60	110	300

10) Pulse-like motions: Would be awesome to show a figure giving this example!
We thank the reviewer for the suggestion. In Figure 6a now we indicate the velocity pulses extracted via wavelet-transform algorithm, superimposed on the velocity time history with a dark line, for two example pulse-like horizontal components. Please see the figure 6.

Figures:
11) I suggest you add a figure showing a map with the distribution of the data, in addition to or instead of the pie chart which is very difficult to interpret.
Done.

12) Also a magnitude-distance plot, which is common in GM databases (see, eg, Ancheta et al, 2014 NGA-West2 database and many other papers).
Magnitude - distance distribution is now reported in Figure 3a.

13) And perhaps a figure to demonstrate Eq. (1), giving that equation as a function of magnitude? (This may help with comment (1) above?).
Done.

14) In general, when referencing figures, I prefer that the prose in the manuscript stands alone, and the figure is simply a support for that, presented parenthetically. For example: You have a great sentence at line 178 where the figure is supporting a statement. An example of a citation that could be improved is at line 216: "Following Anderson (2010) and Pacor et al. (2011b), records with PGAs and PGVs exceeding a given high percentile of the corresponding distributions are identified as extreme (Figure 6)" and then delete the sentence at line 225/226 since that sentence doesn't tell us anything new. Another obvious example is at Line 313. I would suggest (and also suggested some rewording): "A breakdown of pulse-like records by focal mechanism shows an almost-uniform percentage of thirty percent of total near-source ground motions identified as pulse-like (Figure 11). "
Wherever possible, we followed the suggestion of the reviewer.

15) Figure 5: Would be much easier to see your points about the distributions if you showed a histogram or pdf rather than a cdf. Cdf is an unusual way to show this information. Same comment for Figure 14, although in that case the point you are making (that for long periods, the vertical comp. is much smaller) is clear.
Following the papers of Anderson et al (2010) and Pacor et al. (2011), we prefer to maintain this representation.

16) Figure 8, right column: Please add the 10^2 label on the left side of both PGA and PGV plots.
Done.

17) Figure 10: Please state that these records are from the Norcia event
Done. This figure has been moved to Electronic supp.

Line-by-line:

A few grammatical inconsistencies between tenses, agreement, etc. Please proof read carefully.

Line 24: “ever”, not “never”!

Line 54: “… for such effects as a function of a few…”

Line 57: “between”, not “among”.

Line 60: Suggest using the active voice, “To address this issue, we compiled a dataset of near-source strong-motion records, suitable for seismic response analysis and ground motion studies in proximity to the seismic source and accompanied by high-quality metadata, was compiled and it is discussed herein.”

Line 63: “This near-source ground-motion dataset…” (Cut “proposed” and “strong”)

Line 66: Please give the distance restrictions here. Line 70: no need to capitalize “intensity measures.” Also line 89,90.

Line 71: area -> areas

Line 81: lower -> less

Line 86, 87: no need to italicize flat file

Line 142: give the number of earthquakes here.

Line 159: list the 6 distances that you compute.

Line 169: “as a function”

Line 200: What is “T90”? Also do you need references for Housner and Arias?

Line 214: lower à smaller

Line 294: I think you mean to reference Figure 10.

Line 391: I think you mean “NGA-West2”.

We thank the reviewer for the careful revision of the language. We accepted all the suggestions and modified the text accordingly.

NESS1: A worldwide collection of strong-motion data to investigate near-source effects

Francesca PACOR,[1] Chiara FELICETTA, Giovanni LANZANO, Sara SGOBBA, Rodolfo PUGLIA, Maria D'AMICO, Emiliano RUSSO, Georgios BALTZOPOULOS, Iunio IERVOLINO

ABSTRACT

The availability of high-quality waveforms recorded in epicentral areas of moderate-to-strong earthquakes is a key factor for investigating ground-motion characteristics close to the seismic source. In this study, NEar-Source Strong-motion waveforms (*NESS1*) were collected from worldwide public archives with the aim of building a flat-file, available at http://ness.mi.ingv.it, of high-quality metadata and intensity measures of engineering interest. Particular attention was paid to the retrieval of reliable information about event sources, such as geometries and rupture mechanisms, that are necessary to model near-source effects for engineering seismology and earthquake engineering applications. The accelerometric records are manually and uniformly processed and the associated information are fully traceable. NESS1 consists of about 800 three-component waveforms relative to 700 accelerometric stations, caused by 74 events with moment magnitude larger than 5.5 and hypocentral depth shallower than 40 km, with Joyner-Boore distance up to 140 km. Ground motion data were selected to have a maximum source-to-site distance within one fault length, defined through seismological scaling relations.

About 40 records exhibit peak acceleration or peak velocity exceeding 1g or 120 cm/s and they represent some of the largest ground motion ever recorded. Evidence of near-source

[1]Francesca Pacor, Istituto Nazionale di Geofisica e Vulcanologia, Milan, Italy, francesca.pacor@ingv.it

effects was recognized in the NESS1 dataset, such as velocity pulses, large vertical ground motions, directional and hanging-wall amplifications and fling-step. In particular, around 30% of the records were found to exhibit pulse-like characteristics that are possibly due to forward rupture directivity.

Keywords: near-source, source-to-site distance; seismic source; ground-motion intensity.

INTRODUCTION

The availability of waveforms from moderate-to-strong events recorded in epicentral areas is a relevant need for earthquake engineering and engineering seismology purposes. This is demonstrated by the increasing number of studies in the last decades that were focused on the characterization of ground-motion effects in the near-source region, particularly after the 1999 M_W 7.6 Izmit (Turkey) event (e.g., Campbell and Bozorgnia, 2003; Mavroeidis and Papageorgiou, 2003; Somerville, 2003; Bray and Rodriguez-Marek, 2004; Chioccarelli and Iervolino, 2010). These studies pointed out that ground-motion recorded close to the seismic source may show features that are responsible for peculiar seismic demand imposed on structures situated in epicentral area (e.g., Champion and Liel, 2012; Iervolino et al., 2012).

Typical and well-known effects observed in the near-source regions include the vertical component exhibiting much larger amplitude than the corresponding horizontal, pulse-like ground motion due to forward-directivity, *fling-step* effect due to permanent tectonic displacement and hanging-/foot-wall systematic difference. Polarization of motion, or *directionality*, is also observed in strong-motion data recorded close to the source (Shahi and Baker, 2014).

Several attempts have been carried out to model hanging-wall (e.g., Donahue and Abrahamson, 2014) and directivity effects (e.g, Spudich et al., 2014), as well as the amplitude of fling-step (e.g., Faccioli et al., 2004; Kamai et al., 2014; Burks and Baker, 2016). On the other hand, despite the relevant impact and engineering significance of the ground-motion

characteristics in near-source conditions, few attempts have been made to account for them in seismic code provisions (Grimaz and Malisan, 2014; Tothong and Cornell, 2007; Baltzopoulos et al, 2015).

Ground Motion Prediction Equations (GMPEs) typically seek to account for such effects as a function of a few explanatory variables (e.g., magnitude, source-to-site distance, azimuth between the fault-strike and the observer). However, existing models produce results that may significantly differ from one to another, mainly due to the paucity of near-source records and the lack of adequate knowledge and/or high level of uncertainty in the characterization of the fault geometry, which is an essential information to model the mentioned effects.

Another issue concerns the modelling of the distance-scaling in near-source regions, that is only captured by the classical GMPEs up to a some extent, because typical distance-metrics have, in general, limited explanatory power with respect to the effects of the rupture propagation and slip distribution on an extended fault (Thompson and Baltay, 2018).

To contribute in addressing these issues, we compiled a dataset of near-source strong-motion records and metadata, suitable for seismic response analysis and ground-motion studies in proximity to the seismic source. This near-source ground-motion dataset (NEar-Source Strong-motion dataset, version 1.0, or NESS1), is a collection of 800 worldwide records, selected from various repositories of accelerometric data, according to specific criteria in terms of moment magnitude ($M_W \geq 5.5$) and distance. In particular, ground motion data were selected to have a maximum source-to-site distance proportional to the fault length, defined through seismological scaling relations

A fundamental step in the compilation of the NESS1 was to retrieve adequate information about event-source geometries and rupture mechanisms, which allowed the calculation of different metrics to define the source-to-site configuration. Moreover, only raw waveforms available on public repositories were selected and manually processed to construct a

homogeneous dataset of ground motion intensity measures (IMs). The suitability of NESS1 to represent the ground-motion in the near-source is shown by evidence of velocity pulses, large vertical components, polarized ground-motions and hanging-wall effects, that were identified via a preliminary analysis.

DATASET

To construct a dataset of accelerometric waveforms potentially affected by near-source effects, worldwide active crustal earthquakes (Figure 1) were initially selected according to the following criteria: (1) moment-magnitude (M_W) greater than or equal to 5.5; (2) hypocentral depth less than 40 km; (3) availability of geometrical information on the finite fault model; (4) availability of strong-motion records in epicentral area and in free-field conditions.

For the selected events, only raw waveforms were collected, and then uniformly processed to compute the intensity measures. The near-source strong-motion dataset was arranged as a table (named *NESS1 flat-file*) which contains verified and reliable metadata and intensity measures of the manually processed waveforms. The fields of the flat-file are consistent with Engineering Strong Motion flat-file (ESM flat-file, Lanzano et al., 2018) and can be grouped into six main blocks of metadata: (1) event-related; (2) source-related; (3) station-related; (4) metrics of source-to-site distances; (5) waveform-related; (6) ground motion intensity measures. The web page http://ness.mi.ingv.it provides access to the NESS1 flat-file and to related documents (field dictionaries and user manual).

Earthquakes

To build the dataset we identified 74 worldwide events with $M_W \geq 5.5$ (see Table S1, available in the electronic supplement to this article). For 60 earthquakes, fault geometries

were retrieved from published studies or from regional and worldwide databases (see *Data and Resources* section). The saved information includes: strike, dip and rake angles, the depth of the top of rupture plane, the fault length and width, and the coordinates of the reference point that are needed to compute different source-to-site distances. In case of events with multi-segment rupture (e.g., M_W 7.9 2002 Denali, Alaska; M_W 6.6 2011 Fukushima Homadoru, Japan; M_W 7.0 2016 Kumamoto-shi, Japan), the parameters of the dominant fault segment were considered.

Hypocentral coordinates and moment magnitude were recovered after consulting multiple catalogues (see *Data and Resources section*) and specific event studies. For the oldest events, the instrumental hypocenter provided by catalogues may fall beyond the edges of the proposed fault geometry. For this reason, in addition to the coordinates of the instrumental hypocenter, the coordinates of the starting point of the rupture on the fault plane (namely *nucleation point*) were also included.

For other 14 events (Table S1), having high-quality strong-motion records in epicentral area, it was not possible to obtain complete finite source models. In these cases, the strategy of simulating the fault-geometry (*virtual fault,* in Table S1) or some missing parameters was adopted, modifying the procedure by Kaklamanos et al. (2011). The input parameters for virtual fault calculation are the moment magnitude M_W, the strike and dip of the fault plane solutions of moment tensor and the hypocentral depth. The basic steps are: (i) calculation of the fault length L and width W through empirical correlations in function of M_W (Wells and Coppersmith, 1994); (ii) setting the coordinates of the nucleation points equal to hypocentral ones; (iii) computation of the points coordinates of the fault surface projection, assuming the location of the nucleation point at 1/2 L and 2/3 W from the top edge of the fault; (iv) the depth of the top of the fault and the fault trace, obtained from the extension of the fault plane up to surface, are finally calculated accordingly.

The focal mechanism of the events was assigned in accordance to the rake angle of the literature source models or to the solution of the moment tensor provided by the regional and international catalogues, using the convention of Aki and Richards (1980), with the modification of Boore et al. (1997) for strike-slip events.

Strong-motion waveforms

In order to select a number of accelerometric data possibly showing near-source features, it was assumed that such effects occurred in a limited area around the source; i.e., within a few times the fault length. By applying the classical seismological scaling relations (Lay and Wallace, 1995) among seismic moment, slip on the fault and static stress drop $\Delta\sigma$, and the relationship between seismic moment and moment magnitude M_W (Hanks and Kanamori, 1979), a threshold distance R_{ns} (near-source distance), proportional to the fault length was defined as follows:

$$log\ (R_{ns})\ = log\ (k)\ + \frac{1}{2}M_w - \frac{1}{3}log\ (\Delta\sigma)\ + 3.134 \qquad [1]$$

where R_{ns} is given in [m] and $\Delta\sigma$ in [Pa], k is a parameter used to quantify how many fault lengths the sites should be away from the fault, in order to be considered within the region of interest.

The NESS1 dataset features strong-motion data recorded by stations located in the near-source region according to the conventional criterion of [Eq. 1] with k = 1 that is within one fault length, and static stress drop equal to 10 bars; the latter representing the average value for moderate and strong events (Allmann and Shearer, 2009). As the distance metric, the Joyner-Boore distance such as $R_{JB} \leq R_{ns}$ was considered. As an example, the near-source regions for magnitude 6.5 and magnitude 7 earthquakes extend up to 25 km and 40 km,

respectively, from the surface projection of the faults (Figure 2).

The choice of one fault length, although arbitrary, is roughly consistent with evidence of near-source effects in other studies (Chioccarelli and Iervolino, 2010).

Applying the above mentioned criteria to the 74 events, the dataset resulted in 770 waveforms recorded by 666 different accelerometric stations. The majority of the events (Figure 1) are located in United States of America (18 events) and Italy (18 events). Japan and Turkey contribute with 9 and 7 events, respectively. The remaining earthquakes are distributed among Iran (5 events), Greece (5 events), New Zealand (5 events), Montenegro (2 events), Mexico (2 events), Nepal (1 events), Uzbekistan (1 events) and Chile (1 events).

The oldest earthquake included is the well-known M_W 6.4 1933 Long Beach event, that contributes with only a single record to the dataset, while those most recent are the M_W 8.0, 2016, Kaikoura (New Zealand), the M_W 7.0 2016 Kumamoto-shi (Japan) and the M_W 6.5 2016 Norcia (Italy) earthquakes, that are also the most sampled events, with more than thirty waveforms. The event with largest magnitude corresponds to the M_W 8.1 2014 Chilean earthquake.

Source-to-site distance

Close to the seismic source, the point source-to-site distance measures (epicentral and hypocentral distance) that describe the scaling of ground motion intensity are usually replaced by metrics based on the geometry of the finite fault rupture plane. The distance measurements obtained using different metrics can differ significantly, especially in proximity to the source (see Figure S1 available in the electronic supplement to this article). Therefore, for the NESS1 records, six source-to-site distance measurements introduced into the NGA-West2 database (Ancheta et al., 2014) were computed: epicentral distance R_{EPI}, hypocentral distance R_{HYP}, Joyner-Boore distance R_{JB}, rupture distance R_{RUP}, horizontal distance measured perpendicular

to the fault strike R_X, horizontal distance off the surface projection of rupture plane measured parallel to the fault strike R_Y. In addition, the distance from the nucleation point (R_{NP}) and from the top edge of rupture plane (R_{LINE}) were also calculated (Table 2).

Metadata distribution

The dataset covers distances of up to 140 km when measured in R_{JB} terms, with the bulk of records in the magnitude range 6.0 – 7.5 and distances between 0 and 30 km (Figure 2). About half of the waveforms (300) were recorded at R_{JB} < 10 km and 45 waveforms over the surface projection of the fault (R_{JB} = 0).

Normal, strike-slip and thrust focal mechanisms are included in the dataset, with a dominance of strike-slip events mainly located in the United States, New Zealand and Turkey. Normal mechanisms are typical of Italy and Japan, while almost half of the thrust events are located in the United States (see Figure S2, available in the electronic supplement to this article)

Average shear-wave velocity in the uppermost 30 m ($V_{S,30}$) was assigned to all recording stations (Figure S2). When a direct measurement of the S-waves velocity profile was not available, $V_{S,30}$ was estimated by empirical correlation with the topographic slope, as proposed by Wald and Allen (2007) using a 90m DEM (Digital Elevation Map provided by Shuttle Radar Topography Mission). The majority of strong-motion data was recorded on soil ($V_{S,30}$ < 600 m/s), and only 8% on rock sites ($V_{S,30}$ > 800 m/s). In the flat-file, the soil categories relative to the NEHRP (FEMA, 2003) and the EC8 (CEN, 2004) classifications are included, associated using measured VS,30 values, where available (if not, estimated VS,30 is used for the former and surface geological information for the latter).

Waveform processing

The accelerometric data were downloaded from different worldwide databases (see *Data and*

Resources section) in raw version, and manually corrected by using the processing-tool (http://esm.mi.ingv.it/processing/; Puglia et al., 2018) developed within the Engineering Strong Motion Database (ESM; Luzi et al., 2016). This tool implements the procedure described in Paolucci et al. (2011) and detailed in Pacor et al. (2011a) that entails the application of a second-order acausal time-domain Butterworth filter to the zero-padded acceleration time series and zero-pad removal to make acceleration and displacement consistent after double integration.

Most of the digital waveforms, that constitute about 70% of the dataset, are filtered with high-pass frequencies ≥ 0.1 Hz while analog data are, on average, filtered at frequencies around 0.2 Hz due to their lower quality. In both cases, the value of the low-frequency cut-off tends to decrease with increasing magnitude.

For each waveform component (horizontals as-recorded and vertical), peak (peak ground acceleration – *PGA*, peak ground velocity – *PGV*, and peak ground displacement – *PGD*) and integral IMs (significant duration, Housner, and Arias intensities) were computed from the processed waveforms. Furthermore, the 5%-damped acceleration response spectra (*SA*) values are calculated for 36 ordinates in the natural vibration period range 0.01s - 10s.

Several other IMs of horizontal ground motion, such as the geometrical mean, the fault normal (*FN*) and fault parallel (*FP*) components (i.e., normal and parallel to the fault strike) rotated with respect to the fault strike, the maximum (*D100*), the minimum (*D00*), and the median (*D50*) values of the ground motion parameters, were obtained rotating the time series over all orientations (Boore, 2010).

Peak ground motion distributions

The dataset is characterized by relatively large ground-motions: about 50% of the records have horizontal PGAs and PGVs larger than 0.2g and 23 cm/s, while the 2% have PGAs and

PGVs exceeding 1g and 100 cm/s, respectively (Figure 3). The values of the vertical distributions are smaller than the horizontal ones, but tend to increase in the upper percentiles, mainly for high-frequencies ground motion parameters.

Following Anderson (2010) and Pacor et al. (2011b), records with PGAs and PGVs exceeding a given high percentile of the corresponding distributions are identified as *exceptional*. Selecting the 95th percentile as threshold, separately for vertical and horizontal components, 83 such records are recognized within NESS1; 35 of those exceptional records belonging to the 98th percentile of the distribution (Table 2).

The 83 exceptional records mainly come from Japanese, American, New Zealand and Italian events. Strike-slip and thrust earthquakes each account for 89% of this subset, while the remaining 11% is generated by normal fault mechanisms. R_{RUP} of these records varies from 0 to 30 km and they cover the magnitude range 6.0-8.1 (Figure 4).

The exceptional PGAs and PGVs do not seem to exhibit a clear dependence on magnitude and distance, similarly to those observed in previous empirical studies (Anderson, 2010). They may be related to the complexity of the rupture process, such as the localized failure of different portion of the fault (Hanks and Johnson, 1976; Schmedes and Archuleta, 2008). Moreover, site effects can also play a role in ground-motion amplification: in NESS1, exceptional values are mainly recorded on medium-to-dense deposits, characterized by $V_{S,30}$ < 800 m/s and only 7 records are recorded on rock site ($V_{S,30} \geq 800$ m/s). These ground motions were compared with the predictions of the empirical model, proposed by Campbell and Bozorgnia (2014), CB14 hereafter. Indeed, CB14 was calibrated via more than 7,000 data recorded within 80 km from the source and the authors claim (non-regional) applicability to shallow active crustal zones. Although CB14 is calibrated for *D50* as the IM, the residuals (i.e., the difference between natural logarithms of observations and CB14 predictions) were computed considering *D100* values, in order to estimate the deviation of the exceptional

values with respect to the prediction of the reference model. CB14 is able to describe the NESS1 ground motions, as documented by the PGA and PGV residual distributions, that are roughly normally distributed with almost zero median and standard deviations equal to 0.65 and 0.59, respectively (see Figure S3 available in the electronic supplement to this article).

Figure 5 shows the PGA and PGV *epsilons* (i.e., the residual divided by the standard deviation of the prediction model) as a function of magnitude, distance and observed peak parameter. Although no clear trend with magnitude is observed, the majority of the exceptional peak values (black circles) exceeds one standard deviation level and some data points have epsilon larger than 3. Most of the large epsilon values (>2) correspond to the highest PGAs and PGVs included in NESS1; this is evident from Figure 5c, where the number of standard deviations are plotted in functions of the observed peak values.

EVIDENCE OF NEAR-SOURCE EFFECTS IN NESS1

In this section, NESS1 is preliminarily analyzed to recognize some well-known near-source features, such as velocity pulse, large vertical ground motion, directionality and hanging-wall effects. Figure 6 shows some NESS1 processed waveforms, as illustrations of characteristic manifestations of these effects. The velocity waveforms at IT.ACC (M_W 6.5 2016 Norcia event, Italy) and BO.SMN01 (M_W 6.6 2000 Tottori earthquake, Japan) seem to exhibit typical pulse-like behavior. An example of plausible forward directivity can be observed by comparing the *FN* velocity traces recorded at the BO.KMM19 and BO.KMM15 stations (M_W 7.0 2016 Kumamoto-shi earthquake, Japan), that are in opposite positions along the strike direction of the fault: the two velocity waveforms show a different frequency content, with the station that sees most of the rupture propagation happen towards it, i.e., KMM15, exhibiting narrow band, pulse-like characteristics.

Vertical acceleration components exceeding in intensity their horizontal counterparts by a

wide margin, are observed at stations IT.T1214, IT.MRN, situated over the faults of the M_W 6.5 2016 Norcia event and the M_W 6.0 2012 Emilia 2th shock (both Italian). Also interesting is the vertical acceleration trace at BO.IWT33 station (M_W 6.9 2008 Iwate earthquake, Japan), located on the hanging-wall side of the fault. The waveform is asymmetrical and features an extreme PGA value of almost 4g, which is twice the horizontal ones (see Aoi et al., 2008, and Suzuki and Iervolino, 2017, for details). On the other hand, the special position of NZ.WTMC station, close to the epicentre of the M_W 8.0 2016 Kaikoura earthquake (New Zealand), resulted in ground-motion characterized by horizontal PGA exceeding 1.0g on both horizontal components and shorter significant duration with respect to those recorded in the near-source region (Bradley et al., 2017).

Some of the strong motion data included in NESS1 contain the effects of permanent displacement (*PD*), which is notoriously hard to detect using traditional waveform processing methods. Although such static deformation may be significant for near-source records (e.g., *PD* > 10 cm), its estimation entails the adoption of baseline-correction procedures whose details are beyond the scope of this work.

Pulse-like ground motion

In the flat-file compilation, special attention was given to the issue of pulse-like ground motions, due to the engineering relevance of such records. Ground motions with pulse-like characteristics mainly appear when directivity effects combined with the shear-wave radiation pattern lead to constructive wave interference, typically appearing as a double-sided pulse in the velocity signal (Somerville et al., 1997). For the investigation of pulse-like effects within the NESS1 dataset, only records for which instrument orientation was known were considered; i.e., 756 out of the 770 in total. The velocity horizontal records were rotated between 0°-180° and analyzed using the identification algorithm proposed by Baker (2007) to

narrow-down to a subset of candidate impulsive records and to determine pulse period, T_p (Figure 6a). Based on expert judgement, around 230 records were identified and tagged as pulse-like, most likely due to directivity. The relevant metadata of pulse identification tag, pulse period T_p and indicative pulse orientation are included in the NESS1 flat-file, while a detailed account of this investigation is presented in a dedicated study (Baltzopoulos et al., in preparation).

A breakdown of pulse-like records by focal mechanism shows an almost-uniform percentage of thirty percent of total near-source ground motions identified as pulse-like (Figure 7a). A plot of T_p against M_W is also given (Figure 7b), showcasing the well-established positive correlation between pulse duration and magnitude (Mavroeidis and Papageorgiou, 2003; Baker, 2007).

Ground motion components

Considerable vertical ground motions, by virtue of being larger than the corresponding horizontal ones, may appear in waveforms recorded at short distance (Bozorgnia and Campbell, 2004; Bindi et al., 2011; Zafarani et al. 2018). *V/D50,* extracted from NESS1, looks significantly dependent on the natural vibration period *T,* and source-to-site distance (Figure 8a-b): the largest values occur at short periods, with amplitudes close to 1 or even greater at T = 0.1s for sites over the surface projection of the fault (R_{JB} < 1 km). At longer periods, the vertical ground motions are about half of the horizontal one at R_{JB} < 5 km and tend to increase at larger distances, possibly also because of surface waves generated during the propagation.

Near-source effects may also determine the polarization of ground-motions; as a consequence, the ground motion intensity in one orientation can be significantly stronger than in others. For this reason, the geometric mean of the as-measured horizontal ground motion components

may hide some features of the shaking in near-source region. Traditionally, *FN* and *FP* orientations are considered important, as some near-source effects (e.g., long-period velocity pulse in fault-normal, fling in fault-parallel for strike-slip earthquakes) are generally apparent along these orientations (Sommerville, 1997; Mavroeidis and Papageorgiou, 2003). The analysis of NESS1 dataset shows (Figure 8c-d) that the *FN* is larger than *FP* only at long periods (T >1.0s) and in proximity of the fault (R_{JB} < 3 km). Far from the source, these ratios tend to unity, although the scatter around the mean value is large. These results agree with the findings of Watson-Lamprey and Boore (2007), which showed that the maximum ground motions occurred on the *FN* direction only at very short distances.

The *FN*, *FP* and vertical (*V*) ground motion components have similar values at short vibration periods (see Figure S4, available in the electronic supplement to this article); conversely, at intermediate and long periods, the 50th percentile of vertical component is about half of the horizontal ones. Difference between *FN* and *FP* can be appreciated from intermediate (1.0 s) to long periods (3.0 s), where the 50th percentile of *FN* is about 1.5 *FP*.

Since directional effects appear as an important feature of near-source ground-motion, the ratio *D100/D50* as a function of period is also investigated, grouping the data in bins of magnitude (Figure 9a) and distance (Figure 9b). As observed by Boore (2010), this ratio never exceeds 1.42 corresponding to the value expected for linearly polarized ground motion and it is almost independent of distance and magnitude. The largest values are observed at long periods close to the fault plane (R_{JB} < 5 km). This feature, despite distance bins being poorly sampled up to 5 km, might suggest that source contributions, such as radiation pattern and directivity effects, rapidly vanish with distance. These ratios (averaged over all magnitudes and distances) well agree with the predictions of other studies (Shahi and Baker, 2014; Boore and Kishida, 2017) developed using the NGA-WEST2 database in the magnitude range 3 - 8 and distance up to 200 km and the differences do not exceed 4%, when data at R_{jb} < 5 km are

considered (see Figure S4, available in the electronic supplement to this article).

Hanging-/Foot-wall

The hanging-wall effect is defined as the increase in ground-motion at short distances for sites on the hanging wall (*HW*) side of a rupture when compared to sites on the footwall (*FW*) side at equal R_{RUP} (Donahue and Abrahamson, 2014) and it is recognizable in case of dip-slip faults. In NESS1, the waveforms relative to reverse and normal events with $|R_X| < 40$ km and $Ry0 = 0$, were selected to consider only sites located on the projection of the rupture plane. As shown in Figure 10, the high-frequency ground motions (PGA and *SA* at $T < 1.0$ s) exhibit systematically higher values on the hanging wall ($R_X > 0$) than those observed on the footwall side ($R_X < 0$), while no clear dependence on magnitude is observed. On average, the *HW* amplitude is 2 and 1.5 times the *FW* amplitude in the distance range 0 - 16 km for horizontal (Figure 10 a-b) and vertical (Figure 10 c-d) components, respectively.

FINAL REMARKS

The NEar Strong Motion dataset (named NESS1) is composed of about 800 strong motion three-component waveforms relative to about 700 accelerometric stations and caused by 74 events with moment magnitude larger than equal to 5.5 and hypocentral depth shallower than 40 km, recorded in the period time 1933 – 2016. The records were selected with the aim of compile a flat-file of ground-motion parameters and associated metadata (available at http://ness.mi.ingv.it), that can be useful to investigate ground motion characteristics in the proximity of the seismic source. For this reason, accelerometric data observed within one fault length were included in NESS1.

Event and station metadata were manually reviewed by using the most updated national and international catalogues, studies and reports. A fundamental step in the compilation of the dataset was to retrieve reliable information about event sources, such as geometries and

rupture mechanisms, that are key parameters to model relevant near-source effects for engineering applications.

NESS1 only partially overlaps near-source strong-motion data of other published datasets, such as the global NGA-WEST2 database (Ancheta et al., 2014) and the Engineering Strong Motion flat-file (Lanzano et al, 2018), mainly including European events for magnitude 4 and above. About 40% of the NESS1 waveforms are relative to events that occurred in the last five years, thanks to the rapid growth of permanent and temporary networks and the quasi-real time availability of the raw signals in public web repositories (i.e., European Integrated Data Archive EIDA, in DATA and RESOURCE). More than 20% of the data come from normal-faulting events, which are scarcely represented in other global datasets.

A set of preliminary analyses was performed to assess its general representativeness of near-source conditions. First, following previous studies, a subset of records with exceptional peak values was identified. More than 80 records are characterized by peak ground acceleration larger than 0.8g or peak ground velocities in excess of 80 cm/s. The majority of these exceptional values are over one standard deviation above the empirical predictions and some data-points even three times. These data could improve the evaluation of shaking scenarios in epicentral area of strong events, if used to better constrain the maximum expected motions and to identify under which physical conditions they occurred.

Evidence of near-source effects, was recognized in the NESS1 dataset, such as velocity pulses, large vertical ground motions, directional and hanging-wall amplifications and fling-step. These findings substantially confirm existing knowledge from past studies, and in particular the following may be worth highlighting.

1. About 30% of the NESS1 data were found to exhibit pulse-like characteristics over a range of orientations, that are possibly due to rupture directivity. This percentage was almost uniform across focal mechanisms and the estimated pulse periods' scaling with

magnitude was found in agreement with past observations.

2. Differences among the three ground motions components, in terms of peak and spectral accelerations, are observed in proximity of the source and in narrow frequency-band. At short periods, the ratio between vertical to median horizontal ground motion intensity is close to 1 or even greater over the rupture fault, while it is about 1/2 at long periods; at longer distances, the trend is reversed and increases/decreases at long and short periods, respectively. The largest ground motion parameters on fault normal components are only observed at long periods (T > 1.0 s) and very close to the fault plane (R_{JB} < 3 km), where the average ratio between fault normal and fault parallel spectral amplitudes is around 1.5. Finally, the ratio D100/D50 shows a slight dependence on distance, having the largest values close to the source at long periods. The differences with the values predicted by the models of Shahi and Baker (2014) and Boore and Kishida (2017) do not exceed 2%, although the latter are calibrated also including small events and distances up to 200 km.
3. The intensity measures of waveforms recorded in hanging-wall conditions typically exhibit higher values compared to those located in foot-wall at the high-frequencies (T < 1.0 s). These data may be employed to test the simulation-based models for hanging-wall effects.

NESS1 can be a useful tool to investigate the ground shaking in near-source conditions. Further analysis to identify and quantify near-source effects, such as hanging-wall amplification, tectonic fling-step and forward directivity, can contribute to improve the related predictive models for seismic hazard analysis and, ultimately, performance-based earthquake engineering.

ACKNOWLEDGMENTS

This study has been partially developed in the framework of the project RS2: Earthquake Simulations and Near-Source Effects under the agreement DPC-ReLUIS 2014-2018. The Authors are grateful to the project coordinator, Roberto Paolucci, and to Lucia Luzi, coordinator of the European Strong Motion Database, for supporting and encouraging the development of this work. Authors are also thankful to Andrè Herrero for suggesting how to compute the near-source distance. Finally, the authors thank Chiara Maini who contributed to the initial construction of NESS dataset, during her thesis work. The Authors wish to thank Editor, Annemarie Baltay and one anonymous Reviewer for the useful comments and suggestions that improved the quality of our manuscript.

DATA AND RESOURCES

Fault geometries

Fault geometries were obtained from: Database of Individual Seismogenic Sources (DISS, http://diss.rm.ingv.it/diss/); Greek Database of Seismogenic Sources (GreDaSS, http://gredass.unife.it/); Finite-Source Rupture Model Database (Mai et al., 2014; SRCMOD, http://equake-rc.info/SRCMOD/; Next Generation Attenuation relationships for Western US database (NGA-West2, http://peer.berkeley.edu/ngawest2/databases/) and European Strong-Motion Database (ESD, http://www.isesd.hi.is/ESD_Local/frameset.htm).

Hypocentral coordinates and moment magnitude

The locations of the seismic events and the moment magnitudes were obtained from: International Seismological Centre bulletin (ISC, http://www.isc.ac.uk/iscbulletin/); Next Generation Attenuation relationships for Western US database (NGA-West2, http://peer.berkeley.edu/ngawest2/databases/); Istituto Nazionale di Geofisica e Vulcanologia (INGV) bulletin (http://webservices.rm.ingv.it/fdsnws/event/1/); European–Mediterranean

Seismological Centre bulletin (EMSC, http://www.seismicportal.eu/fdsnws/event/1/); United States Geological Survey (USGS, http://earthquake.usgs.gov/); GeoNet-New Zealand seismic catalogue (http://quakesearch.geonet.org.nz/); Center for Engineering Strong Motion Data - (CESMD, http://strongmotioncenter.org/); ING Catalogue (1450 b.C. - 1990); *Catalogo della Sismicità Italiana* 1981-2002, versione 1.1 (CSI, http://www.ingv.it/CSI/); *Bollettino Sismico Italiano, Istituto Nazionale di Geofisica e Vulcanologia - Centro Nazionale Terremoti* (http://bollettinosismico.rm.ingv.it/); Global Centroid-Moment Tensor Catalog (GCMT, http://www.globalcmt.org/CMTsearch.html); United States Geological Survey (USGS, http://earthquake.usgs.gov/); EMSC-CSEM webservice (http://www.emsc-csem.org/Bulletin/); European-Mediterranean Regional Centroid-Moment Tensors Catalog (RCMT, http://www.bo.ingv.it/RCMT/);

Waveforms

Accelerometric time series were obtained from different online databases: GeoNet seismic catalog (https://www.geonet.org.nz/) for New Zealand; Strong-motion Seismograph Networks of National Research Institute for Earth Science and Disaster Resilience (http://www.kyoshin.bosai.go.jp/) for Japan; Unified HEllenic Accelerogram Database (HEAD, http://www.itsak.gr/en/head or http://accelnet.gein.noa. gr) for Greece; ITalian ACcelerometric Archive (ITACA, http://itaca.mi.ingv.it) for Italy; the National Strong-Motion Network of Turkey (TR-NSMN, http://kyhdata.deprem.gov. tr/2K/kyhdata_v4.php); Strong-motion Virtual Data Center (http://strongmotioncenter.org/); United States Geological Survey (https://earthquake.usgs.gov/); California Geological Survey (http://www.quake.ca.gov/); , and Engineering strong motion database (ESM, http://esm.mi.ingv.it).

REFERENCE

Aki, K., and P.G. Richards (1980). Quantitative Seismology. University Science Books.

Allmann, B.P., and P.M. Shearer (2009). Global variations of stress drop for moderate to large earthquakes, Journal of geophysical Research, 114, B01310, doi:10.1029/2008JB005821.

Ancheta, T.D., R.B. Darragh, J.P. Stewart, E. Seyhan, W.J. Silva, B.S.J. Chiou, K.E. Wooddell, R.W. Graves, A.R. Kottke, D.M. Boore, T. Kishida, and J.R. Donahue (2014). NGA-West2 Database. Earthq Spectra 30 (3): 989–1005.

Anderson, J.G. (2010). Source and site characteristics of earthquakes that have caused exceptional ground accelerations and velocities. Bulletin of the Seismological Society of America 100(1): 1–36, February 2010, doi: 10.1785/0120080375

Aoi, S., T. Kunugi and H. Fujiwara (2008). Trampoline Effect in Extreme Ground Motion. Science. 322(5902): 727-730 DOI: 10.1126/science.1163113

Atkinson, G. M., E. Yenier, N. Sharma, and V. Convertito (2016). Constraints on the near-distance saturation of ground-motion amplitudes for small-to-moderate induced earthquakes. Bulletin of the Seismological Society of America, 106(5), 2104-2111.

Baker, J.W. (2007). Quantitative classification of near-fault ground motions using wavelet analysis, Bull. Seism. Soc. Am., 97 (5): 1486-1501.

Baltzopoulos, G., C. Eugenio, and I. Iervolino (2015). The Displacement Coefficient Method in near-Source Conditions. Earthquake Engineering and Structural Dynamics 44(7): 1015–33.

Bindi, D., F. Pacor, L. Luzi, R. Puglia, M. Massa, G. Ameri, and R. Paolucci (2011). Ground motion prediction equations derived from the Italian strong motion database, Bull. Seism. Soc. Am.9 1899-1920.

Bindi, D., M. Massa, L. Luzi, G. Ameri, F. Pacor, R. Puglia, and P. Augliera. (2014). Pan-European ground-motion prediction equations for the average horizontal component of PGA, PGV, and 5%-damped PSA at spectral periods up to 3.0 s using the RESORCE dataset. Bulletin of earthquake engineering, 12(1), 391-430.

Boore D.M., and T. Kishida (2017). Relations between some horizontal-component ground motion intensity measures used in practice. Bull. Seismol. Soc. Am., 107 (1): 334-343. doi:10.1785/0120160250

Boore, D. M. (2010). Orientation-independent, non geometric-mean measures of seismic intensity from two horizontal components of motion, Bull. Seismol. Soc. Am. 100, 1830–1835.

Bozorgnia, Y., and K.W. Campbell (2004). The vertical-to-horizontal spectral ratio and tentative procedures for developing simplified V/H and vertical design spectra, J. Earthq. Eng. 4, no. 4, 539–561.

Bradley, BA., H.N.T. Razafindrakoto, and V. Polak (2017). Ground-Motion Observations from the 14 November 2016 Mw 7.8 Kaikoura, New Zealand, Earthquake and Insights from Broadband Simulations. Seismological Research Letters Volume 88, Number 3 May/June 2017

Bray, J.D., and A. Rodriguez-Marek (2004) Characterization of forward-directivity ground motions in the near-fault region. Soil Dynamics and Earthquake Engineering; 24(11):815–828.

BSSC (2003) NEHRP recommended provisions for seismic regulations for new buildings and other structures (fema 450)

Burks, L.S., and J.W. Baker (2016). A predictive model for fling-step in near-fault ground motions based on recordings and simulations. Soil Dynamics and Earthquake Engineering. Vol. 80, 119-126.

Campbell, K.W., and Y. Bozorgnia (2003) Updated Near-Source Ground-Motion (Attenuation) Relations for the Horizontal and Vertical Components of Peak Ground Acceleration and Acceleration Response Spectra. Bulletin of the Seismological Society of America; 93(1): 314–331.

Campbell, K.W., and Y. Bozorgnia (2014). NGA-West2 ground motion model for the average horizontal components of PGA, PGV, and 5% damped linear acceleration response spectra. Earthquake Spectra, 30(3), 1087-1115.

CEN (Comite Européen de Normalisation) (2004), Eurocode 8: Design of structures for earthquake resistance – Part 1: General rules, seismic actions and rules for buildings. CEN European Committee for Standardization.

Champion, C., and A. Liel (2012). The effect of near-fault directivity on building seismic collapse risk. Earthquake Engineering Structural Dynamics. Vol 40(10): 1391 - 1409. https://doi.org/10.1002/eqe.1188

Chioccarelli, E., and I. Iervolino (2010) Near-source seismic demand and pulse-like records: a discussion for L'Aquila earthquake. Earthquake Eng Struct. Dyn.; 39:1039–1062.

Cotton, F., and M. Campillo. 1995. Frequency-Domain Inversion of Strong Motions - Application to the 1992 Landers Earthquake. J. Geophys. Res.,100 (B3):3961-3975.

Donahue, J.L., and N.A. Abrahamson (2014). Simulation-Based Hanging Wall Effects. Earthquake Spectra, Volume 30, No. 3, pages 1269–1284.

Faccioli, E., R. Paolucci, and J. Rey (*2004*) Displacement Spectra for Long Periods. Earthquake Spectra: 20(2), 347-376.

Gregor, N., N.A. Abrahamson, G.M. Atkinson, D.M. Boore, Y. Bozorgnia, K.W. Campbell, and W. Silva (2014). Comparison of NGA-West2 GMPEs. Earthquake Spectra, 30(3), 1179-1197.

Grimaz, S., and P. Malisan (2014) Near field domain effects and their consideration in the international and Italian seismic codes. Boll. Geof. Teor. Appl., vol. 55, n.4, pp. 717-738.

Hanks, T.C., and H. Kanamori (1979). A moment magnitude scale. Journal of Geophysical Research, 84, 2348-2350.

Hanks, T.C, and D.A. Johnson (1976). Geophysical assessment of peak accelerations. Bulletin of the Seismological Society of America. Vol. 66, No. 3, pp. 959 968.

Iervolino, I., E. Chioccarelli, and G. Baltzopoulos (2012) Inelastic displacement ratio of near-source pulse-like ground motions. Earthquake Engineering and Structural Dynamics, 41:2351–2357.

Kamai, R., N. Abrahamson, and R. Gaves (2014). Adding Fling Effects to Processed Ground-Motion Time Histories. Bulletin of the Seismological Society of America, Vol. 104, No. 4, pp. 1914–1929, doi: 10.1785/0120130272

Kaklamanos, J., L.G. Baise, and D.M. Boore (2011). Estimating unknown input parameters when implementing the NGA ground-motion prediction equations in engineering practice. Earthquake Spectra, 27 (4), 1219-1235.

Lay T., and T. Wallace (1995). Modern Global Seismology. Academic Press, 521 pp.

Luzi, L., F. Pacor, R. Puglia, G. Lanzano, C. Felicetta, M. D'Amico, M. Michelini, L. Faenza, V. Lauciani, I. Iervolino, G. Baltzopoulos, and E. Chioccarelli (2017). The Central Italy Seismic Sequence between August and December 2016: Analysis of Strong-Motion Observations. Seismological Research Letters Volume 88, Number 5 September/October 2017. doi: 10.1785/0220170037

Luzi, L., R. Puglia, E. Russo and ORFEUS WG5 (2016). Engineering Strong Motion Database, version 1.0. Istituto Nazionale di Geofisica e Vulcanologia, Observatories & Research Facilities for European Seismology. doi: 10.13127/ESM

Lanzano, G., S. Sgobba, L. Luzi, R. Puglia, F. Pacor, C. Felicetta, M. D'Amico, F. Cotton, and D. Bindi (2018). The pan-European Engineering Strong Motion (ESM) flatfile: compilation criteria and data statistics. Bulletin of Earthquake Engineering (submitted).

Mai, M., and K.K.S. Thingbaijam (2014). SRCMOD: An Online Database of Finite-Fault Rupture Models. Seismological Research Letters 85 (6) 1348-1357, doi: 10.1785/0220140077.

Mavroeidis, G.P., and A.S. Papageorgiou (2003) A mathematical representation of near-fault ground motions. Bulletin of the Seismological Society of America; 93(3):1099–1131

Pacor, F., R. Paolucci, G. Ameri, M. Massa, and R. Puglia (2011a). Italian strong motion records in ITACA: overview and record processing. Bull Earthquake Eng (2011) 9:1741–1759 DOI 10.1007/s10518-011-9295-x

Pacor, F., R. Paolucci, L. Luzi, F. Sabetta, A. Spinelli, A. Gorini, M. Nicoletti, S. Marcucci, L. Filippi, and M. Dolce (2011b). Overview of the Italian strong motion database ITACA 1.0. Bull Earthquake Eng 9 (6): 1723–1739. doi: 10.1007/s10518-011-9327-6.

Paolucci, R., F. Pacor, R. Puglia, G. Ameri, C. Cauzzi, M. Massa (2011). Record processing in ITACA, the new Italian strong-motion database, in Earthquake Data in Engineering Seismology-Predictive Models, Data Management and Networks, S. Akkar, P. Gülkan, and T. van Eck (Editors), Springer, Dordrecht, Netherlands, 99–113, ISBN: 978-94-007-0151-9 (printed version) 978-94-007-0152-6 (e-book version).

Puglia, R., E. Russo, L. Luzi, M. D'Amico, C. Felicetta, F. Pacor, and G. Lanzano (2018). Strong-motion processing service: a tool to access and analyse earthquakes strong-motion waveforms. Bull. Earthquake Eng. https://doi.org/10.1007/s10518-017-0299-z

Schmedes, J., and R.J. Archuleta (2008). Near-source ground motion along strike-slip faults: Insights into magnitude saturation of PGV and PGA. Bulletin of the Seismological Society of America, 98(5), 2278-2290.

Shahi S., and J.W. Baker (2014). NGA-West2 models for ground-motion directionality. Earthq Spectra 30, 1285-1300.

Somerville, P.G. (2003) Magnitude scaling of the near fault rupture directivity pulse. Physics of the Earth and Planetary Interiors; 137:201–212.

Somerville, P.G., N.F. Smith, R.W. Graves, and N.A. Abrahamson (1997). Modification of empirical strong ground motion attenuation relations to include the amplitude and duration effects of rupture directivity, Seismological Research Letters 68, 199-222.

Spudich, P., B. Rowshandel, S.K. Shahi, J.W. Baker, and B.S.J. Chiou (2014). Comparison of NGA-West2 directivity models, Earthq. Spectra, 30(3), 1199–1221.

Suzuki A., and I. Iervolino (2017) Italian vs worldwide history of largest PGA and PGV. Annals of Geophysics, 60(5), S0551. doi: 10.4401/ag-7391.

Thompson, E.M. and Baltay, A.S. The Case for Mean Rupture Distance in Ground Motion Estimation. Submitted to Bulletin of the Seismological Society of America (June 2018).

Tothong, P., C.A. Cornell, and J.W. Baker (2007) Explicit directivity-pulse inclusion in probabilistic seismic hazard analysis. Earthq. Spectra 23, 867–891.

Wald, D.J., and T.I. Allen (2007). Topographic slope as a proxy for seismic site conditions and amplification. Bulletin of the Seismological Society of America, 97 (5), 1379-1395.

Watson-Lamprey, J. A., and D. M. Boore (2007). Beyond SaGMRotI: Conversion to SaArb, SaSN, and SaMaxRot, Bull. Seism. Soc. Am. 97, 1511-1524. (1.6 Mb)

Wells, D.L., and Coppersmith K.J. (1994). New empirical relationships among magnitude, rupture length, rupture width, rupture area, and surface displacement. Bulletin of the Seismological Society of America, 84 (4), 974-1002.

Zafarani, H., L. Luzi, G. Lanzano, M.R. Soghrat (2017). Empirical equations for the prediction of PGA and pseudo spectral accelerations using Iranian strong-motion data. Journal of Seismology (pre-print), DOI:10.1007/s10950-017-9704-y.

AUTHORS

Francesca Pacor, Istituto Nazionale di Geofisica e Vulcanologia, Milan, Italy, francesca.pacor@ingv.it

Chiara Felicetta, Istituto Nazionale di Geofisica e Vulcanologia, Milan, Italy, chiara.felicetta@ingv.it

Giovanni Lanzano, Istituto Nazionale di Geofisica e Vulcanologia, Milan, Italy, giovanni.lanzano@ingv.it

Sara Sgobba, Istituto Nazionale di Geofisica e Vulcanologia, Milan, Italy, sara.sgobba@ingv.it

Rodolfo Puglia, Istituto Nazionale di Geofisica e Vulcanologia, Milan, Italy, rodolfo.puglia@ingv.it

Maria D'Amico, Istituto Nazionale di Geofisica e Vulcanologia, Milan, Italy, maria.damico@ingv.it

Emiliano Russo, Istituto Nazionale di Geofisica e Vulcanologia, Centro Nazionale Terremoti, Rome, Italy, emiliano.russo@ingv.it

Georgios Baltzopoulos, Dipartimento di Strutture per l'Ingegneria e l'Architettura, Università degli Studi di Napoli Federico II, Naples, Italy, georgios.baltzopoulos@unina.it

Iunio Iervolino, Dipartimento di Strutture per l'Ingegneria e l'Architettura, Università degli Studi di Napoli Federico II, Naples, Italy, iunio.iervolino@unina.it

TABLES

Table 1. Notation and description of the distance measures.

Distance measures	**Description**
R_{EPI}	Epicentral distance: distance from epicentre
R_{HYP}	Hypocentral distance: distance from hypocentre
R_{JB}	Joyner-Boore distance: distance computed from the surface projection of the fault
R_{RUP}	Rupture distance: shorter distance to the rupture plane
R_X	Horizontal distance measured perpendicular to the fault strike, from the top edge of rupture plane
R_{Y0}	Horizontal distance off the surface projection of rupture plane, measured parallel to the fault strike.
R_{NP}	Nucleation point distance: distance from nucleation point
R_{LINE}	Shorter distance from the top edge of rupture plane, computed as $\sqrt{R_X^2+R_{Y0}^2}$

Table 2. List of the 35 exceptional records (sorted by time) within NESS1. Data belonging to the 98th percentile of the peak ground motion (PGA or PGV) distribution for D100 and vertical components are highlighted in grey. Network code, station code, $V_{S,30}$ values, event-ID, event name, event data-time, moment magnitude (M_W), focal mechanism (FM), rupture distance (R_{RUP}), Joyner-Boore distance (R_{JB}) are reported. $V_{S,30}$ estimation methods are from: V_S profile (VS), geological features (GEO) and topographic proxy (TOPOG).

Net-code	Station code	$V_{S,30}$ [m/s]	$V_{S,30}$ method	Event-ID	Event name	Event data-time	M_W	FM	R_{RUP} [km]	R_{JB} [km]	D100-PGA [cm/s2]	D100-PGV [cm/s]	V-PGA [cm/s2]	V-PGV [cm/s2]
CE	24207	800.0	TOPOG	USGS-iscgem787038	San Fernando	'1971-02-09 14:00:40'	6.7	TF	4.44	3.27	1436.79	119.09	672.89	54.25
A	GZL	327.8	TOPOG	UZ-1976-0001	Gazli	'1976-05-17 02:58:41'	6.7	TF	5.28	3.67	708.03	63.17	1186.73	61.65
M	E060	203.2	VS	USGS-usp00013ee	Imperial Valley	'1979-10-15 23:16:57'	6.5	SS	1	0.1	436.54	119.11	1549.34	57.06
M	5051	348.7	VS	USGS-usp0003afe	Superstition Hills	'1987-11-24 13:15:56'	6.6	SS	1	0.65	492.78	155.70	444.68	32.05
TK	2402	580.0	TOPOG	TK-1992-0002	Erzican	'1992-03-13 17:18:39'	6.6	SS	1	0.85	478.19	127.60	240.83	13.81
M	5453	580.0	TOPOG	USGS-usp00066k9	Northridge	'1994-01-17 12:30:54'	6.7	TF	13.52	4.64	796.05	141.96	468.20	18.55
M	5451	580.0	TOPOG	USGS-usp00066k9	Northridge	'1994-01-17 12:30:54'	6.7	TF	15.75	0.13	495.44	119.57	469.62	23.31
CE	24514	580.0	TOPOG	USGS-usp00066k9	Northridge	'1994-01-17 12:30:54'	6.7	TF	5.22	1.51	860.37	132.07	535.88	19.43
CE	24279	269.0	VS	USGS-usp00066k9	Northridge	'1994-01-17 12:30:54'	6.7	TF	5.95	3.22	736.06	120.03	575.74	33.01
M	5450	580.0	TOPOG	USGS-usp00066k9	Northridge	'1994-01-17 12:30:54'	6.7	TF	18.97	16.04	674.89	98.83	872.41	27.69
CE	24436	257.0	VS	USGS-usp00066k9	Northridge	'1994-01-17 12:30:54'	6.7	TF	15.75	0.13	1782.53	123.00	1059.30	74.88
CE	24207	800.0	TOPOG	USGS-usp00066k9	Northridge	'1994-01-17 12:30:54'	6.7	TF	6.82	4.64	1645.64	107.36	1310.93	50.65
A	496	800.0	TOPOG	TK-1999-0415	Duzce	'1999-11-12 16:57:19'	7.3	SS	4.32	0.1	1073.13	43.30	317.37	16.71
BO	TTR02	310.0	VS	JP-2000-0007	Tottori	'2000-10-06 04:30:17'	6.6	SS	1.1	0.98	1107.49	143.47	775.78	56.19
I1	BAM	499.0	VS	IR-2003-0041	Bam	'2003-12-26 01:56:53'	6.5	SS	1.47	0.1	838.61	123.27	962.55	39.84
CE	36456	246.0	VS	USGS-nc51147892	Parkfield	'2004-09-28 17:15:24'	6	SS	2.51	0.24	1268.79	89.00	562.52	23.50
BO	NIG15	405.0	VS	JP-2004-0002	Niigata 1st shock	'2004-10-23 08:55:58'	6.6	TF	11.35	10.09	1692.09	66.50	550.76	13.48
BO	NIG13	372.0	VS	JP-2004-0002	Niigata 1st shock	'2004-10-23 08:55:58'	6.6	TF	8.83	0.1	1502.73	132.43	758.23	28.20
BO	IWT34	371.0	VS	EMSC-20080613_0000091	Iwate	'2008-06-13 23:43:46'	6.9	TF	5.53	5.49	1138.79	57.05	910.70	28.10
BO	IWT33	506.0	VS	EMSC-20080613_0000091	Iwate	'2008-06-13 23:43:46'	6.9	TF	5.09	0.1	1387.43	71.30	3702.31	86.19
NZ	HORC	394.4	TOPOG	EMSC-20100903_0000044	Darfield	'2010-09-03 16:35:46'	7.1	SS	7.24	7.24	533.04	103.70	653.26	60.17
NZ	LINC	358.0	TOPOG	EMSC-20100903_0000044	Darfield	'2010-09-03 16:35:46'	7.1	SS	7.57	5.38	484.11	116.16	779.84	76.91
NZ	GDLC	403.1	TOPOG	EMSC-20100903_0000044	Darfield	'2010-09-03 16:35:46'	7.1	SS	1.08	1.08	786.94	151.44	1006.78	39.60
NZ	HPSC	207.0	VS	EMSC-20110221_0000047	Christchurch 1st shock	'2011-02-21 23:51:42'	6.2	TF	4.25	4.22	256.10	41.18	1008.00	34.86

NZ	D07C	283.0	TOPOG	EMSC-20110221_0000047	Christchurch 1st shock	'2011-02-21 23:51:42'	6.2	TF	3.92	3.89	724.17	74.83	1517.58	44.49
NZ	HVSC	352.0	VS	EMSC-20110221_0000047	Christchurch 1st shock	'2011-02-21 23:51:42'	6.2	TF	3.35	0.1	1470.31	98.96	1612.63	41.64
NZ	PRPC	192.0	VS	EMSC-20110221_0000047	Christchurch 1st shock	'2011-02-21 23:51:42'	6.2	TF	2.83	2.79	731.35	122.81	1822.04	49.34
NQ	KATNP	580.0	TOPOG	EMSC-20150425_0000021	Nepal	'2015-04-25 06:11:26'	7.8	TF	9.61	0.1	160.52	111.18	179.51	58.29
BO	KMM16	580.0	TOPOG	USGS-us20005iis	Kumamoto-shi	'2016-04-15 16:25:06'	7	NF	4.72	0.1	574.58	61.63	387.54	55.84
BO	KMM10	280.0	VS	USGS-us20005iis	Kumamoto-shi	'2016-04-15 16:25:06'	7	NF	1	0.1	1307.30	141.53	869.51	52.38
IT	CLO	420.5	TOPOG	EMSC-20161030_0000029	Norcia	'2016-10-30 06:40:18'	6.5	NF	1.92	0.1	590.28	69.62	782.02	68.62
NZ	KIKS	374.6	TOPOG	EMSC-20161113_0000048	Kaikoura	'2016-11-13 11:02:58'	8	SS	3.49	0.1	252.46	86.36	242.58	62.33
NZ	KEKS	786.3	TOPOG	EMSC-20161113_0000048	Kaikoura	'2016-11-13 11:02:58'	8	SS	18.78	1.58	1294.38	116.03	338.87	69.01
NZ	WDFS	378.8	TOPOG	EMSC-20161113_0000048	Kaikoura	'2016-11-13 11:02:58'	8	SS	20.67	4.8	1253.87	107.75	384.39	54.60
NZ	WTMC	529.2	TOPOG	EMSC-20161113_0000048	Kaikoura	'2016-11-13 11:02:58'	8	SS	11.99	0.1	1103.51	119.88	1993.14	46.90

LIST OF FIGURE CAPTIONS

Figure 1. Map of the epicentral distribution of the 74 worldwide earthquakes included in NESS1.

Figure 2. Data-distribution of NESS1: magnitude, MW, versus Joyner-Boore distance, RJB. Lines represent the scaling of the near-source distance in function of magnitude and stress drop according to Eq .1 and k = 1 (a) waveforms number as a function of M_W (b) and Joyner-Boore distance, R_{JB} (c).

Figure 3. Empirical cumulative distribution functions for *PGA* (a) and *PGV* (b) in terms of *D100* (solid lines) and vertical component (dashed lines). The reported values 1073 cm/s^2 and 870 cm/s^2 for PGA, as well as 119 cm/s and 52 cm/s for PGV indicate the upper 2th percentiles. Mean and standard deviation (log10 unit) are also reported.

Figure 4. Magnitude (a-b) and distance (c-d) scaling of D100 PGAs (a-c) and PGVs (b-d) included in NESS1. The Exceptional values are indicated by squares.

Figure 5. Number of standard deviation, epsilon, above and below the CB14 median predictions for PGA (a-b-c) and PGV (d-e-f) of NESS1 dataset (grey circles) and the exceptional data (black circles), plotted in function magnitude (a-d), rupture distance (b-e) and observed peak values (c-f). D100 values are used in the plots.

Figure 6. Examples of acceleration/velocity waveforms exhibiting evidence of near-source effects. Station code and component orientation are reported together with the moment magnitude M_W and the rupture distance R_{RUP}. PGA and PGV values are also listed. (a) Pulse-like velocity traces recorded at IT.ACC station (M_W 6.5 2016 Norcia event, Italy) and BO.SMN01 station (M_W 6.6 2000 Tottori earthquake, Japan) and wavelet representation (Baker, 2007) of the velocity pulse (black thick line); (b) velocity traces (fault-normal components) recorded at two stations, BO.KMM15 and BO.KMM19, that were found in diametrically opposed positions with respect to the fault rupture of the M_W 7.0 2016 Kumamoto-shi event (Japan); (c) vertical acceleration components recorded at station IT.MRN during the M_W 6.0 2nd shock of the 2012 Emilia sequence and IV.T1214 during the M_W 6.5 20016 Norcia event; (d) Fault-normal horizontal acceleration component recorded at NZ.WTMC during the M_W 8.0 2016 Kaikoura earthquake (New Zealand) and vertical acceleration component recorded at BO.IWT33

during the M_W 8.0 2008 Iwate earthquake (Japan).

Figure 7. a) Breakdown of pulse-like records identified within the NESS1 dataset by focal mechanism in histogram format (right): bins of records belonging to strike-slip (SS), thrust faulting (TF), normal faulting (NF) events; b) Pulse period versus moment magnitude plot.

Figure 8. Ratios of Vertical (V) to D50 for spectral ordinates SA at T = 0.1 (a) and 3.0 s (b) versus Joyner and Boore distance; ratios of fault-normal (FN) to fault-parallel (FP) for PGA (c) and spectral ordinates SA at T= 3.0s (d). The number of data in each bin is reported.

Figure 9. a) D100/D50 ratios for all records and for three magnitude bins, as well as all magnitude bins combined (all magnitudes, the same as $5 \leq MW \leq 8$); b) D100/D50 ratios for all records and for three distance (RJB) bins, as well as all distance bins combined (all distance, the same as $0 \leq RJB \leq 140$ km). For each period, the D100/D50 is computed as the geometric mean of the ratios for each observation. The bars represent the 95% confidence of the mean. The NESS1 data-trend is compared with the models of Boore and Kishida (2017) and Shahi and Baker (2014).

Figure 10. *PGA* and *SA* at 0.3 s distributions as function of R_X distance for sites on the hanging-wall (*HW*, $R_X > 0$) and footwall (*FW*, $R_X < 0$). a-b: horizontal component; c-d: vertical component. The number of data in each bin is reported.

FIGURES

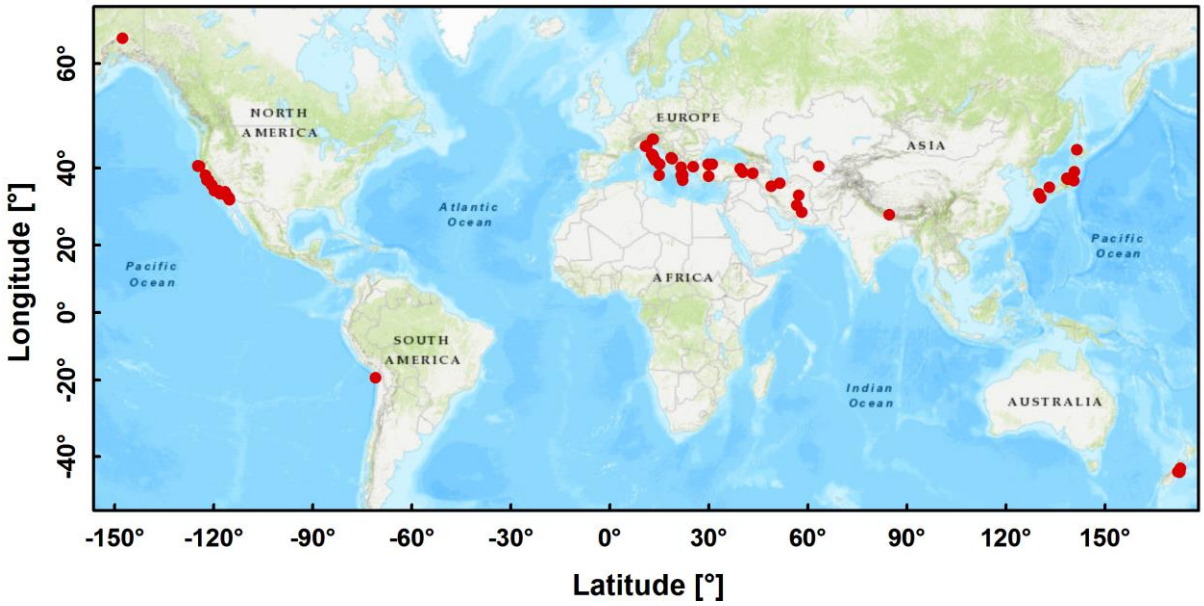

Figure 1. Map of the epicentral distribution of the 74 worldwide events included in NESS.

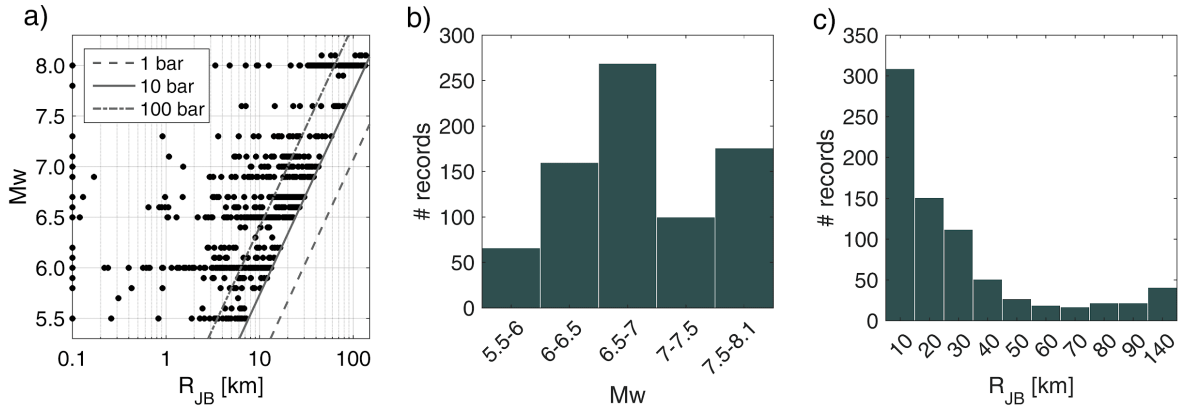

Figure 2. Data-distribution of NESS1: magnitude, M_W, versus Joyner-Boore distance, R_{JB}. Lines represent the scaling of the near-source distance in function of magnitude and stress drop according to Eq .1 and k = 1 (a) waveforms number as a function of M_W (b) and Joyner-Boore distance, R_{JB} (c).

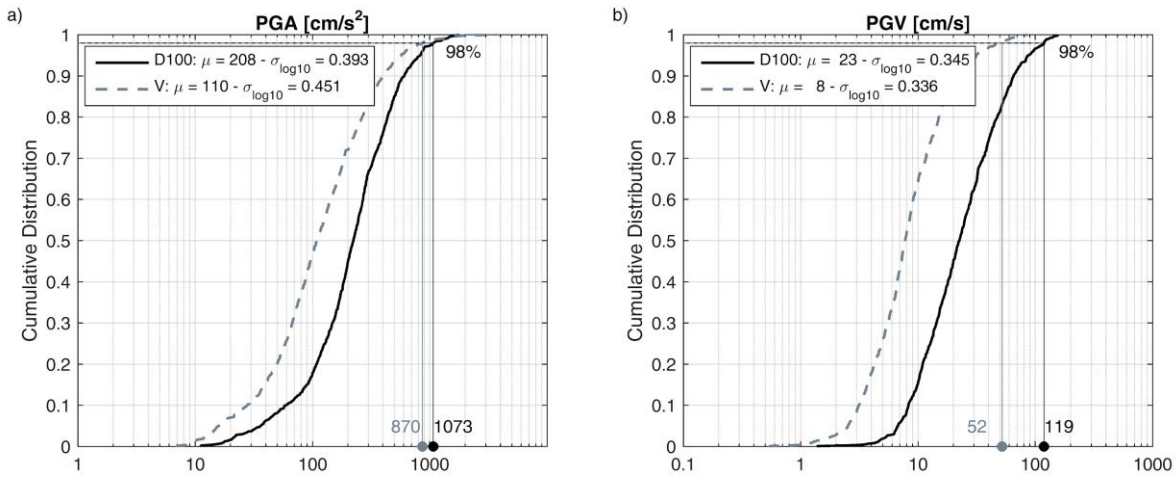

Figure 3. Empirical cumulative distribution functions for *PGA* (a) and *PGV* (b) in terms of *D100* (solid lines) and vertical component (dashed lines). The values of the upper 2th percentiles, are reported. Mean and standard deviation (log10 unit) of the distributions are also reported.

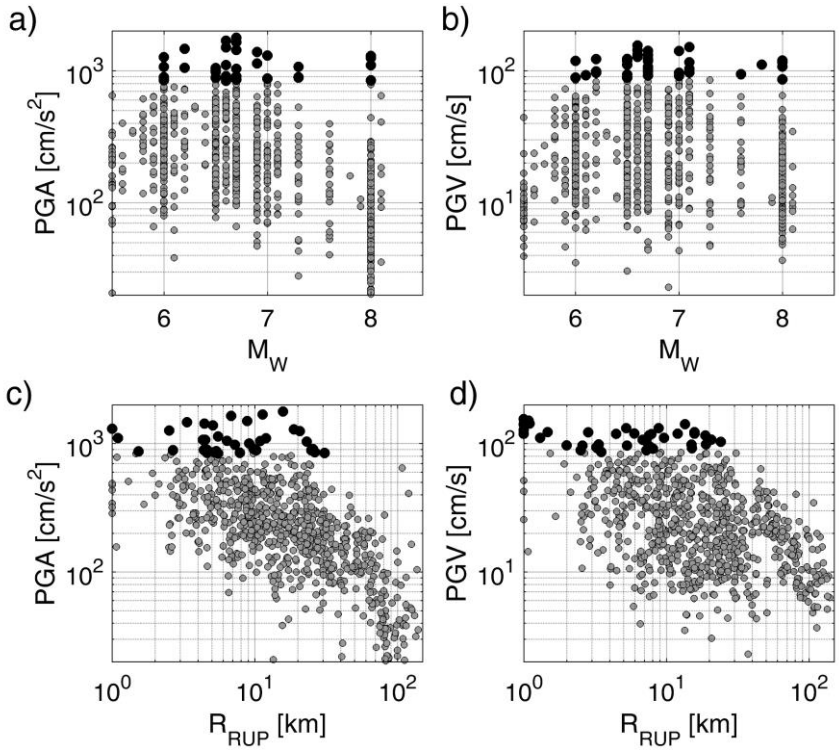

Figure 4. Magnitude (a-b) and distance (c-d) scaling of D100 PGAs (a-c) and PGVs (b-d) included in NESS1. The Exceptional values are indicated by squares.

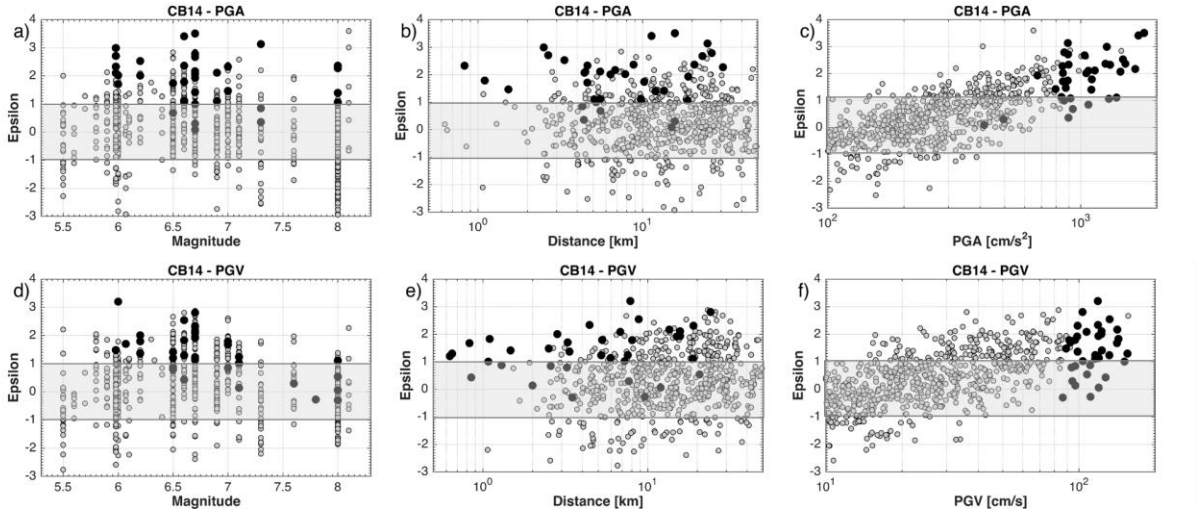

Figure 5. Number of standard deviation, epsilon, above and below the CB14 median predictions for PGA (a-b-c) and PGV (d-e-f) of NESS1 dataset (grey circles) and the exceptional data (black circles), plotted in function magnitude (a-d), rupture distance (b-e) and observed peak values (c-f). D100 values are used in the plots.

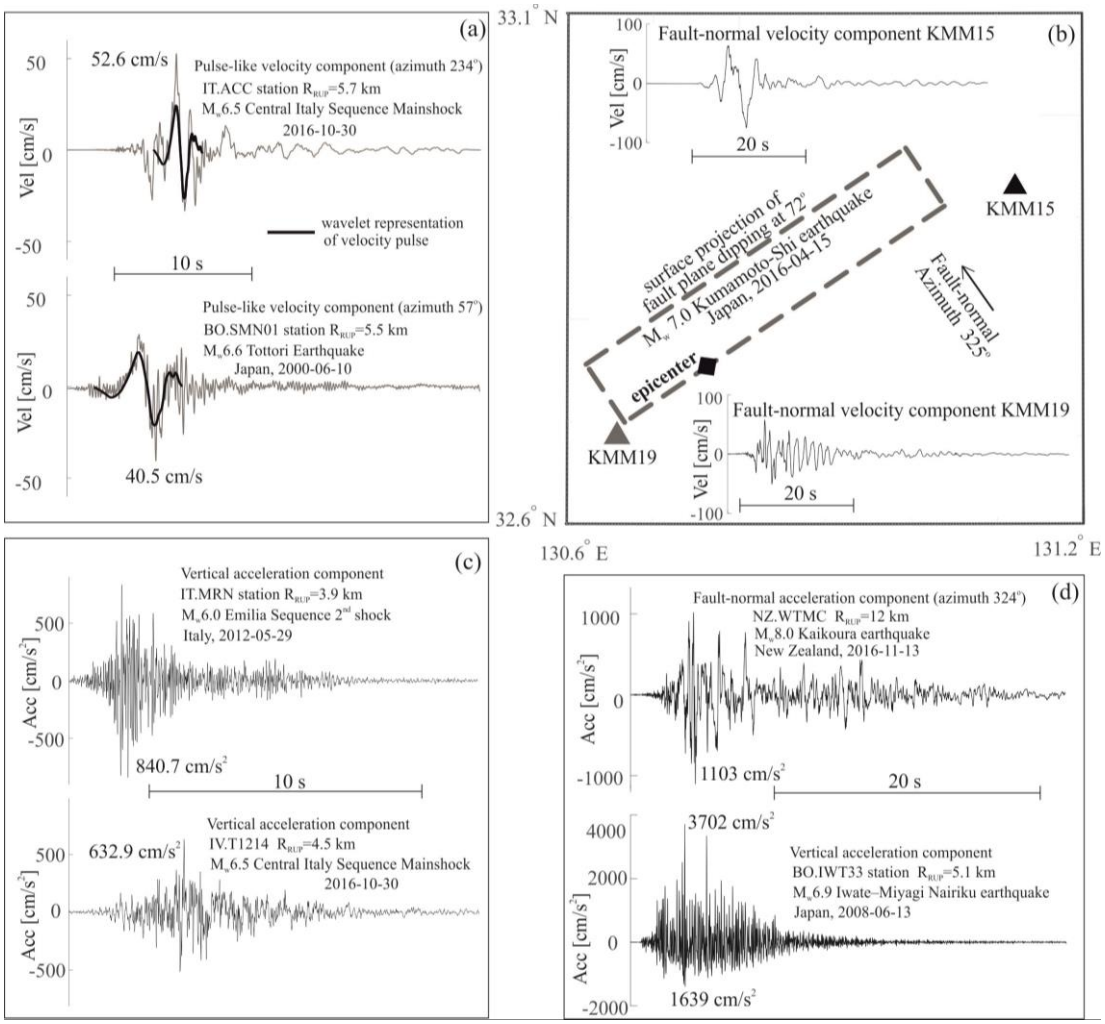

Figure 6. Examples of acceleration/velocity waveforms exhibiting evidence of near-source effects. Station code and component orientation are reported together with the moment magnitude M_W and the rupture distance R_{RUP}. PGA and PGV values are also listed. (a) Pulse-like velocity traces recorded at IT.ACC station (M_W 6.5 2016 Norcia event, Italy) and BO.SMN01 station (M_W 6.6 2000 Tottori earthquake, Japan) and wavelet representation (Baker, 2007) of the velocity pulse (black thick line); (b) velocity traces (fault-normal components) recorded at two stations, BO.KMM15 and BO.KMM19, that were found in diametrically opposed positions with respect to the fault rupture of the M_W 7.0 2016 Kumamoto-shi event (Japan); (c) vertical acceleration components recorded at station IT.MRN during the M_W 6.0 2nd shock of the 2012 Emilia sequence and IV.T1214 during the M_W 6.5 20016 Norcia event; (d) Fault-normal horizontal acceleration component recorded at NZ.WTMC during the M_W 8.0 2016 Kaikoura earthquake (New Zealand) and vertical acceleration component recorded at BO.IWT33 during the M_W 8.0 2008 Iwate earthquake (Japan).

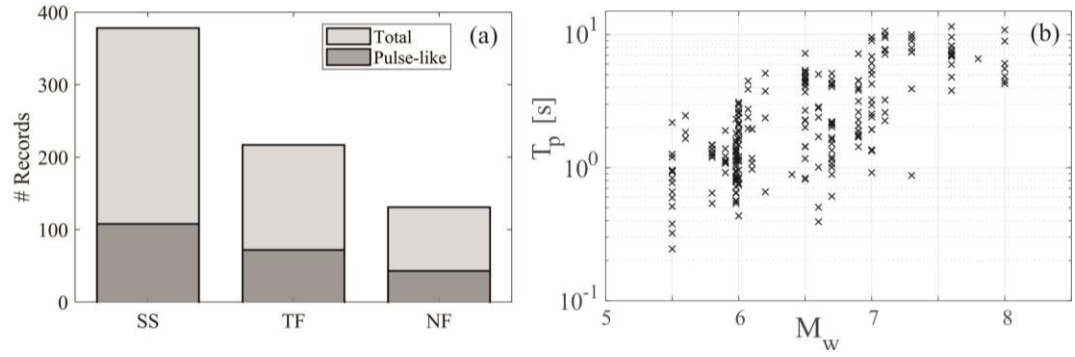

Figure 7. a) Breakdown of pulse-like records identified within the NESS1 dataset by focal mechanism in histogram format (right): bins of records belonging to strike-slip (SS), thrust faulting (TF), normal faulting (NF) events; b) Pulse period versus moment magnitude plot.

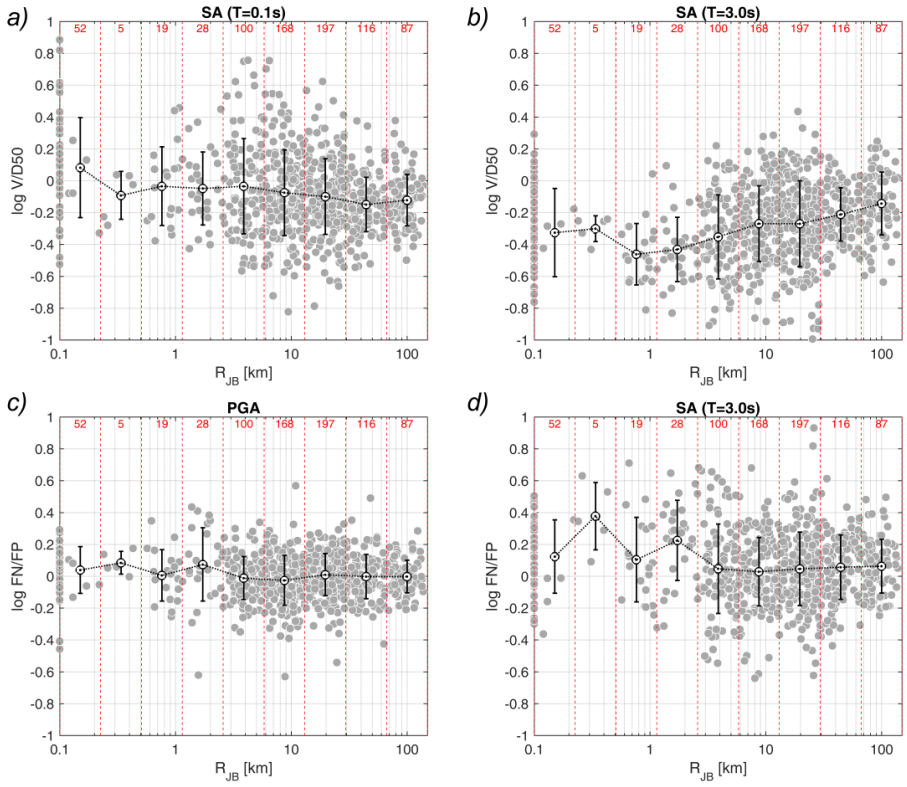

Figure 8. Ratios of Vertical (V) to D50 for spectral ordinates SA at T = 0.1 (a) and 3.0 s (b) versus Joyner and Boore distance; ratios of fault-normal (FN) to fault-parallel (FP) for PGA (c) and spectral ordinates SA at T= 3.0s (d). The number of data in each bin is reported.

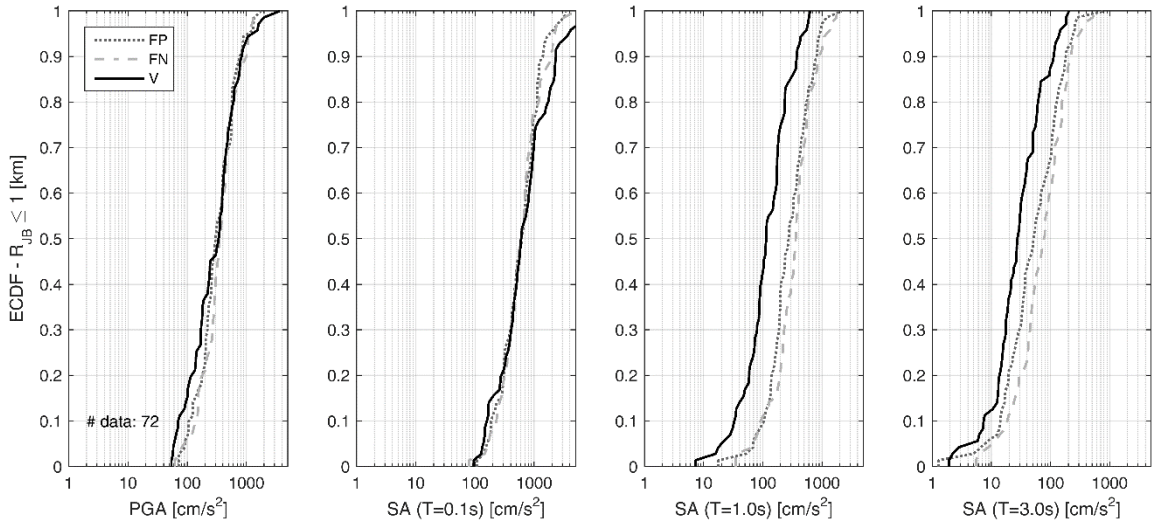

Figure 9. Cumulative distributions of different IMs (*PGA*, *SA* at 0.1, 1.0 and 3.0 s) observed at distances $R_{JB} \leq 1$ km for Fault-Parallel (*FP*, dotted line), Fault-Normal (*FN*, dashed line), and vertical (*V*, solid line) components. Number of data is also reported.

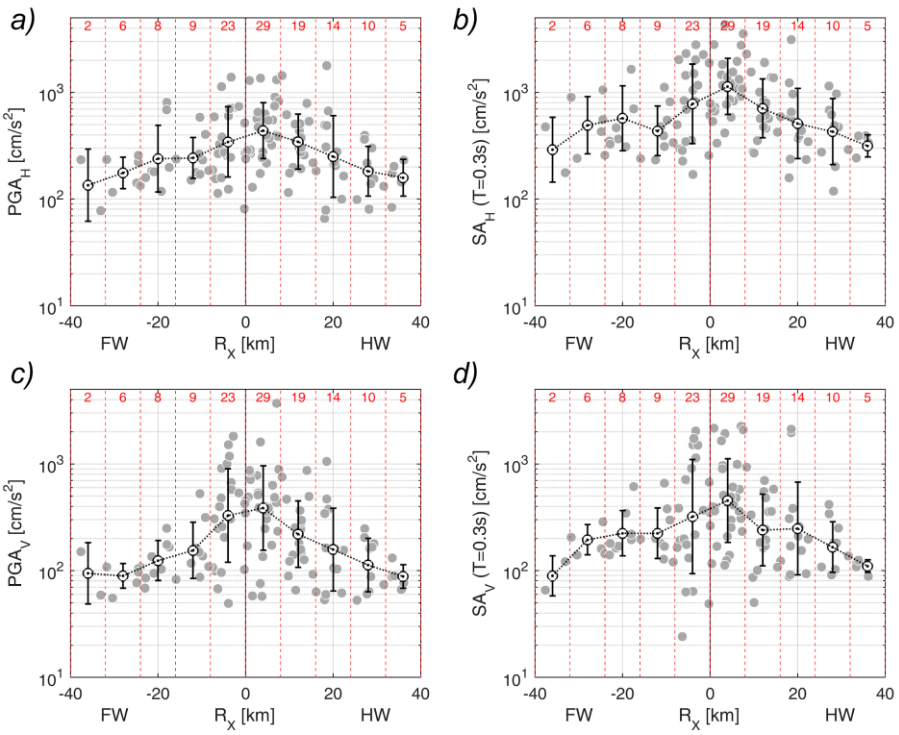

Figure 10. *PGA* and *SA* at 0.3 s distributions as function of R_X distance for sites on the hanging-wall (*HW*, $R_X > 0$) and footwall (*FW*, $R_X < 0$). a-b: horizontal component; c-d: vertical component. The number of data in each bin is reported.

Figure_1

Click here to download Figure Figure_1.png

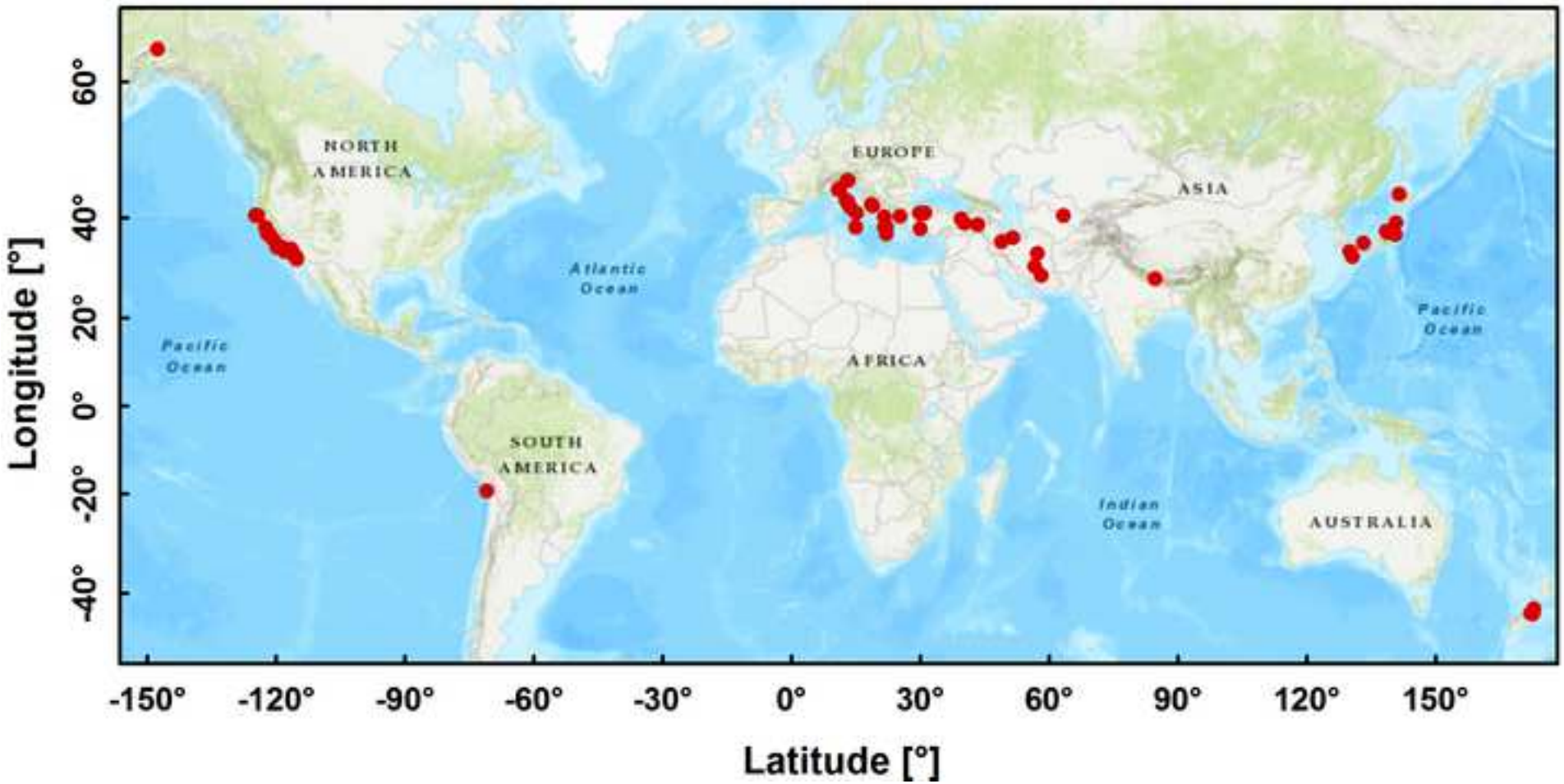

Figure_2

Click here to download Figure Figure_2.png

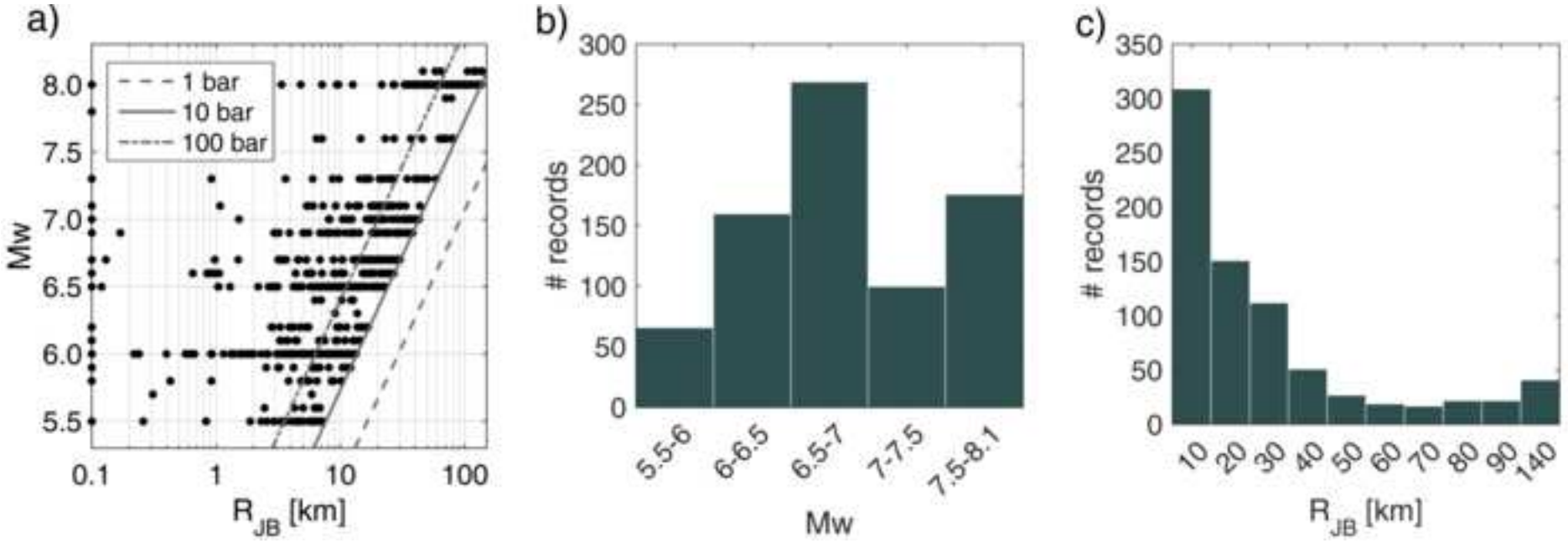

Figure_3

Click here to download Figure Figure_3.png

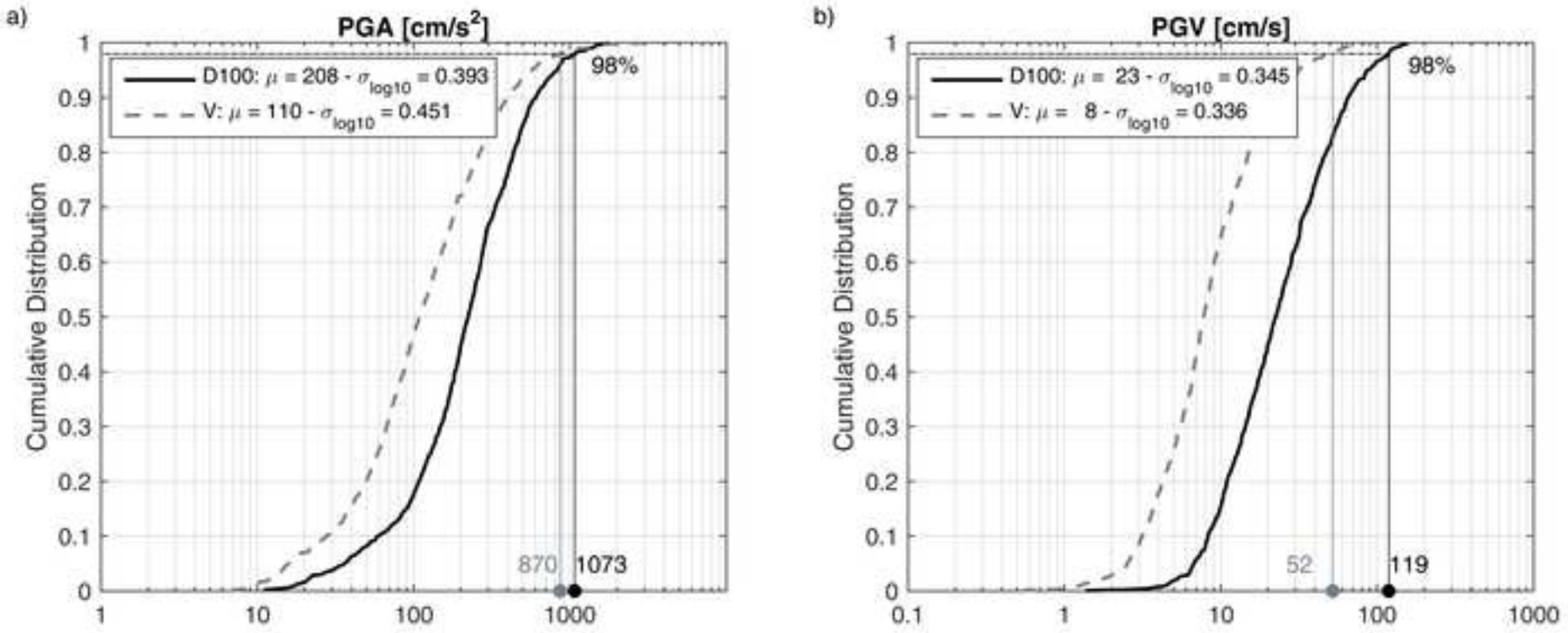

Figure_4

Click here to download Figure Figure_4.png

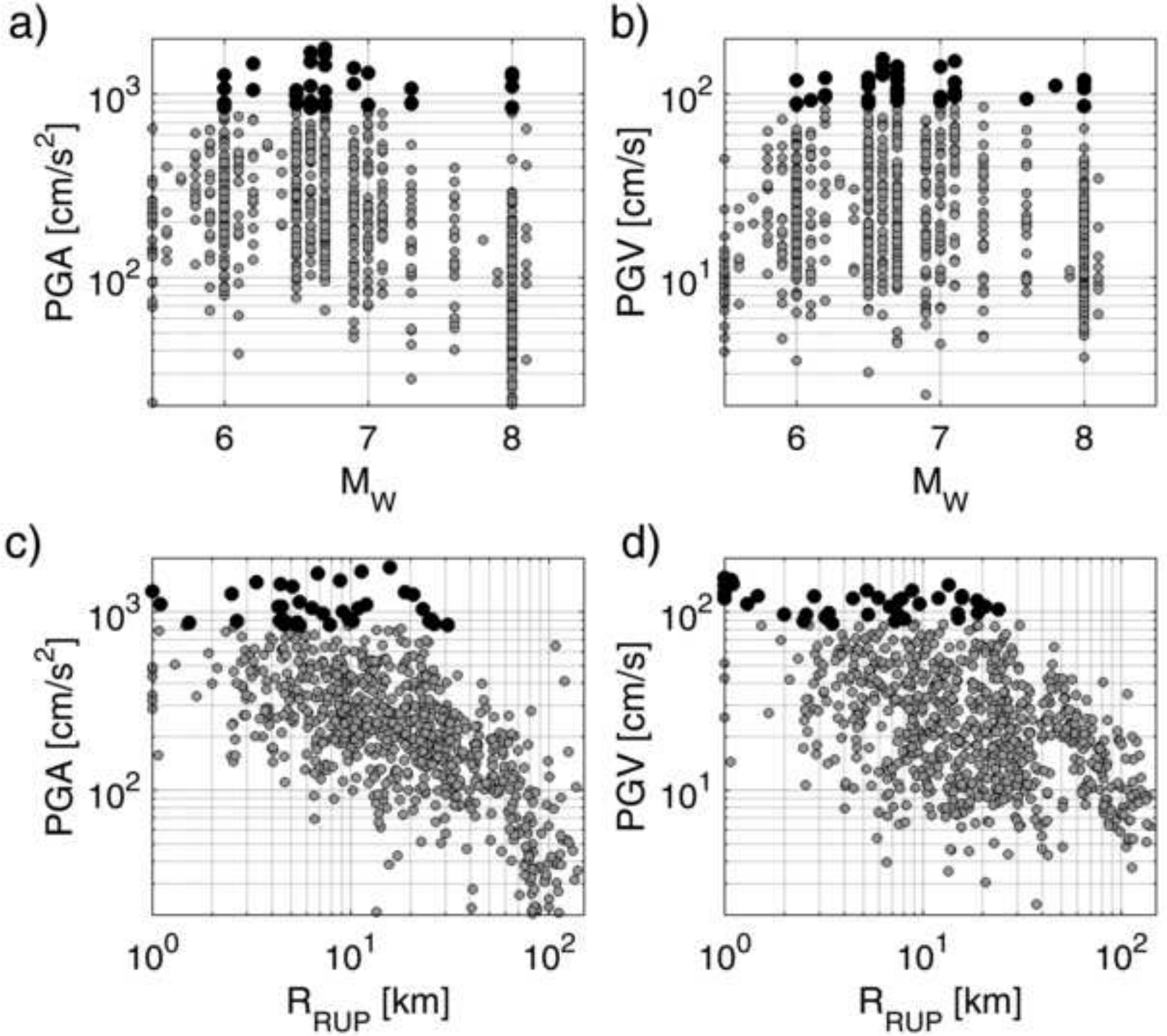

Figure_5

Click here to download Figure Figure_5.png

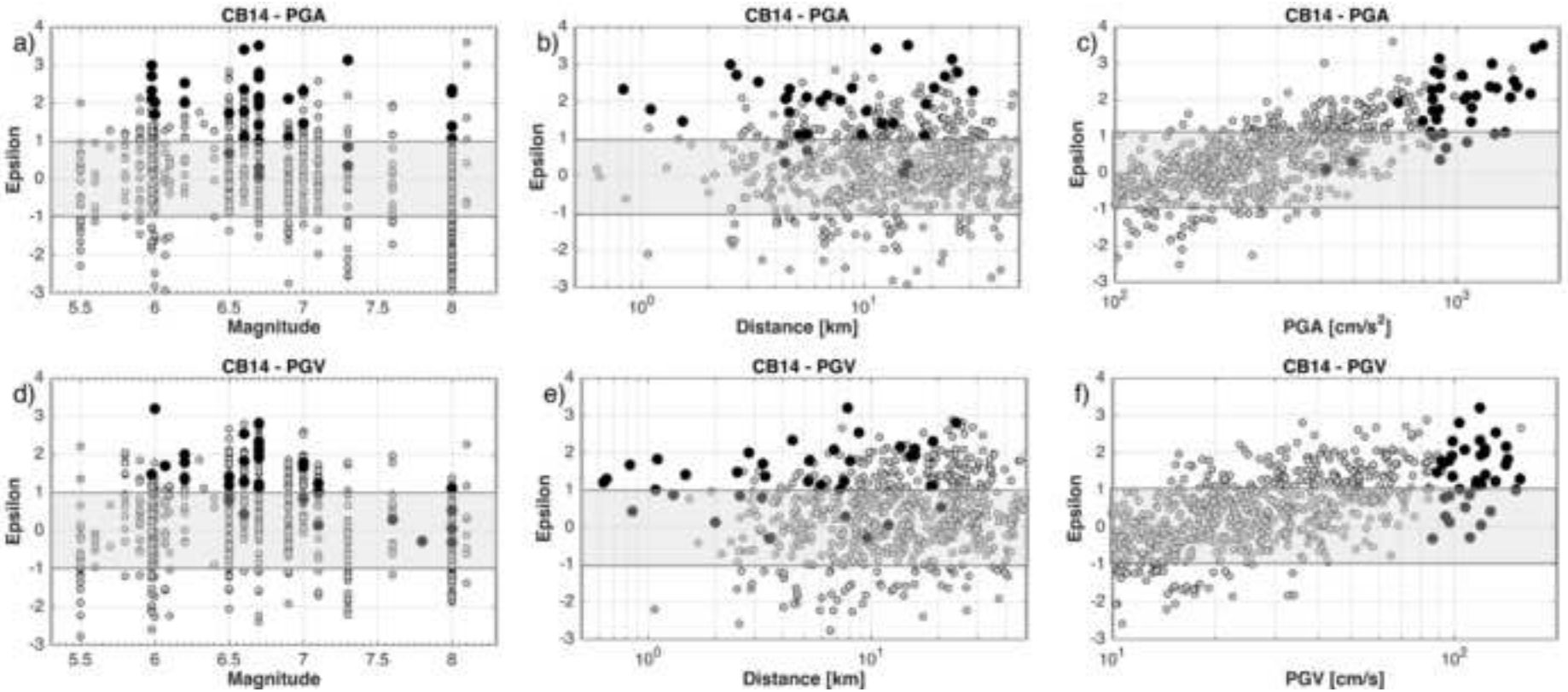

Figure_6

Click here to download Figure Figura_6.jpg

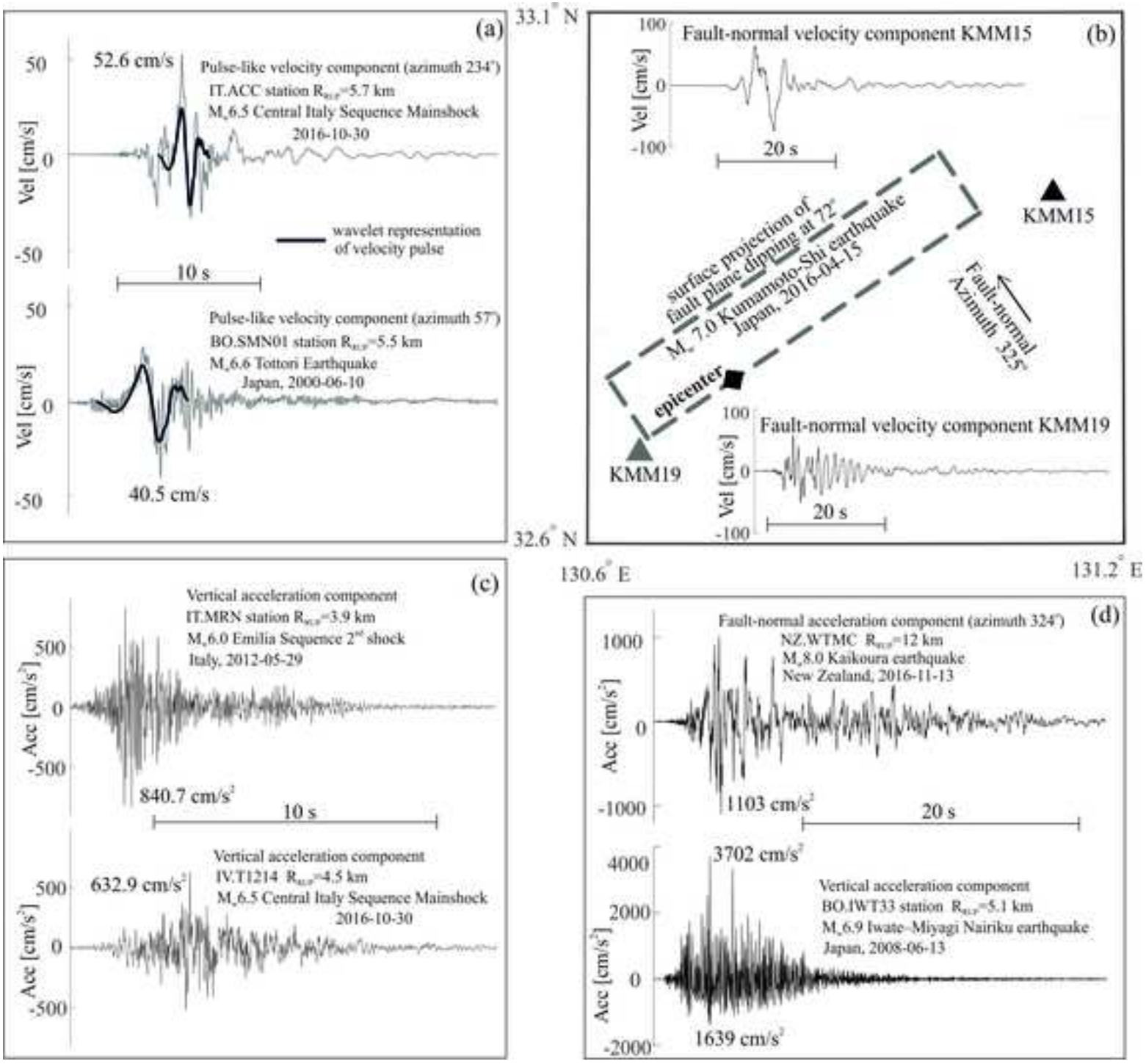

Figure_7

Click here to download Figure Figura_7.jpg

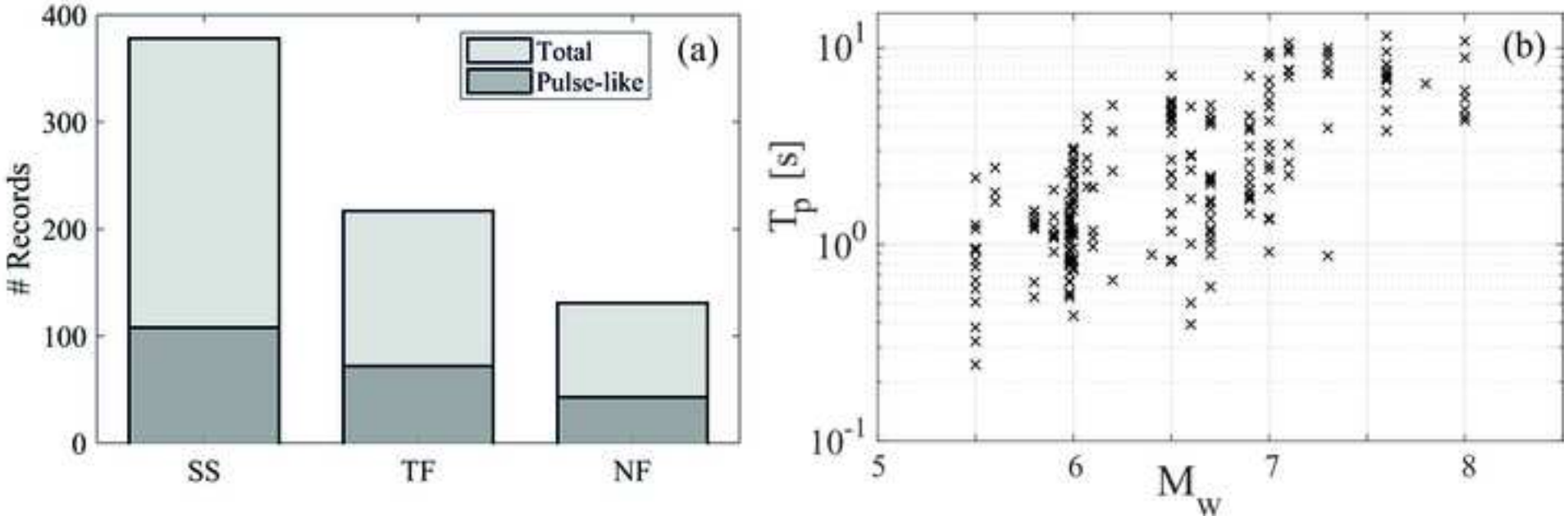

Figure_8

Click here to download Figure Figure_8.png

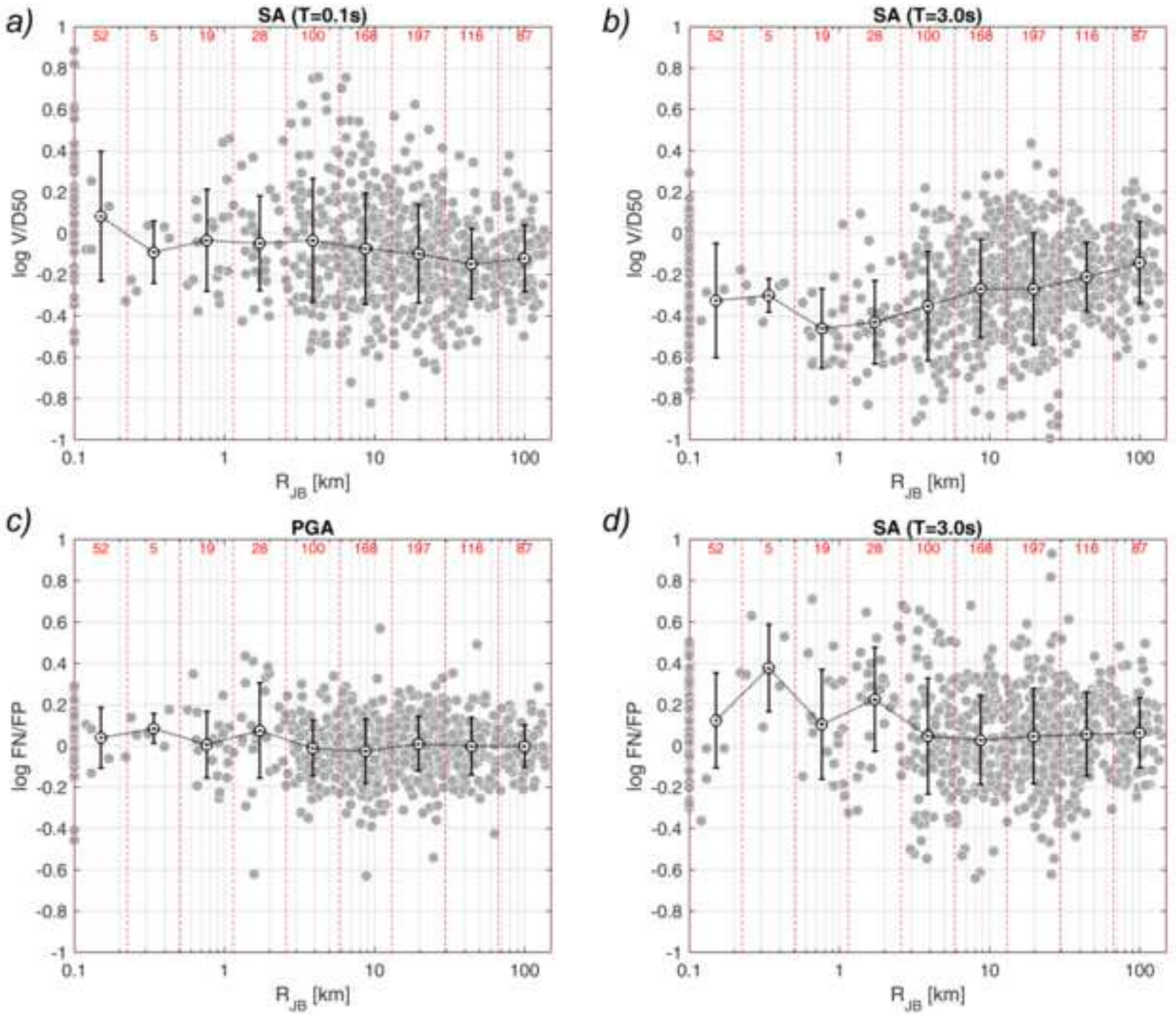

Figure_9

Click here to download Figure Figure_9.png

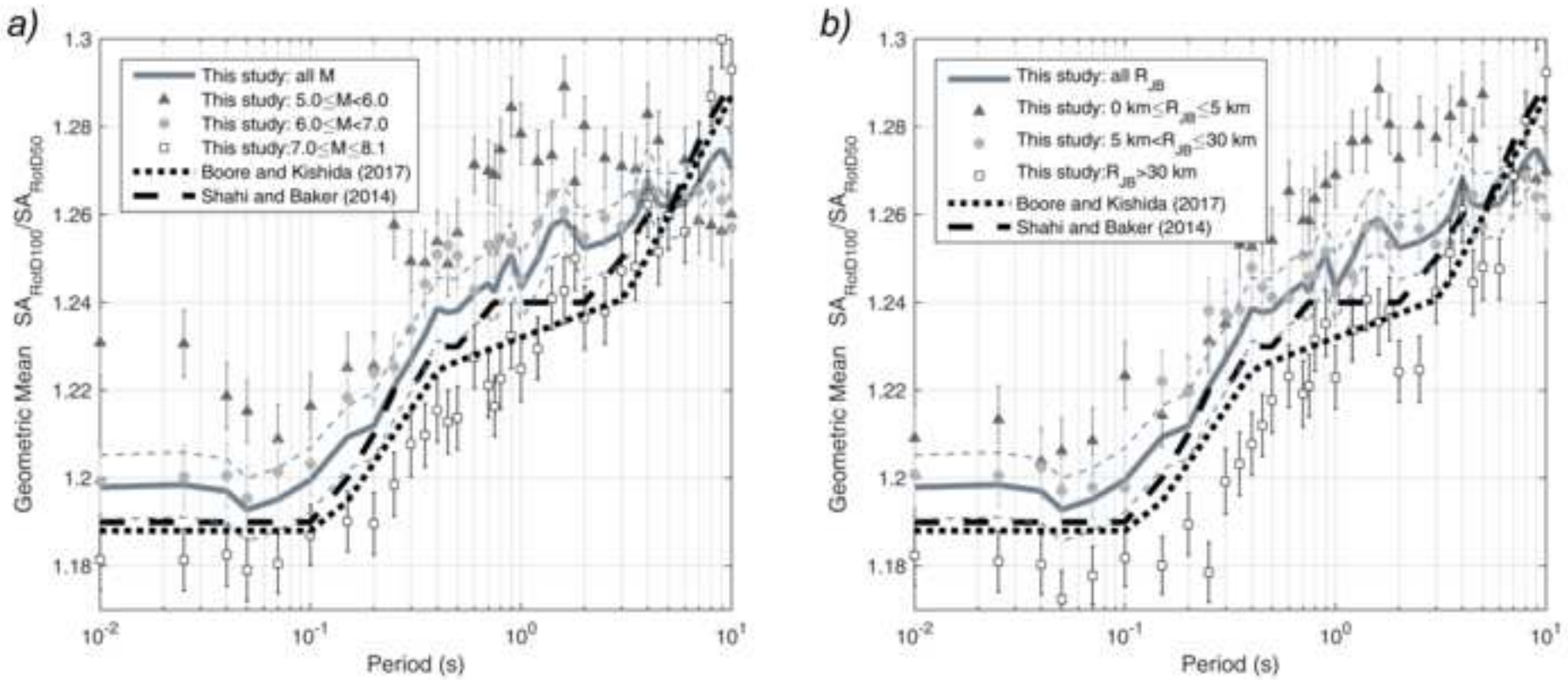

Figure_10

Click here to download Figure Figure_10.png

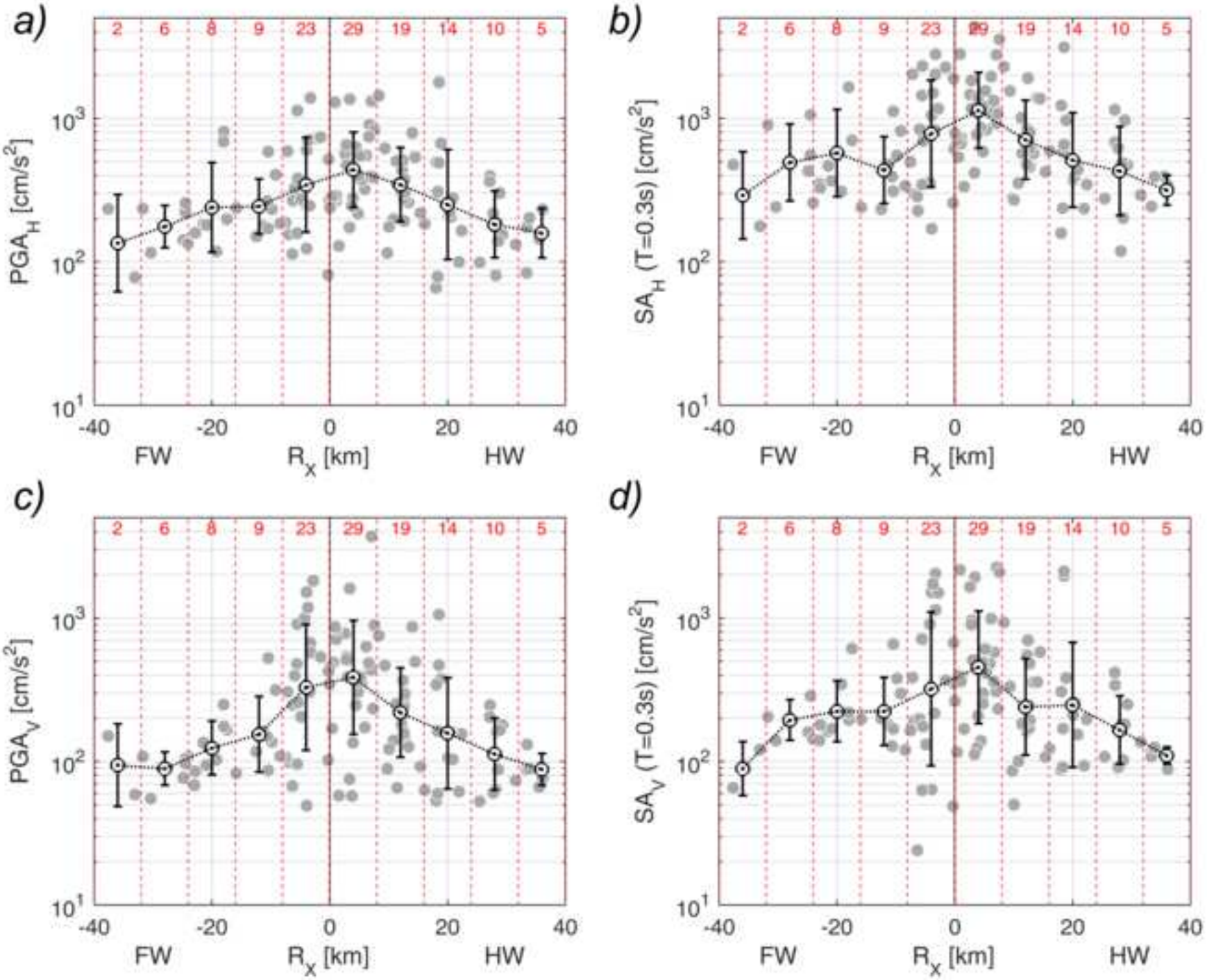

NESS v1.0: A worldwide collection of strong-motion data to investigate near source effects

Francesca PACOR[1], Chiara FELICETTA, Giovanni LANZANO, Sara SGOBBA, Rodolfo PUGLIA, Maria D'AMICO, Emiliano RUSSO, Georgios BALTZOPOULOS, Iunio IERVOLINO

Metadata

Supplemental material provides adding information on NEar-Source Strong motion dataset. Table S1 lists the main features of the selected events, including the references of fault geometry parameters.

Figure S1 shows how the metrics (rupture distance, R_{RUP}, line distance, R_{LINE} and nucleation distance, R_{NP}, defined in Table 1 of the main text) differ in the proximity of the source (R_{JB} < 1km). In these plots, the Joyner-Boore distance is considered as the reference metric, because it is widely adopted in the calibration of GMPEs.

Figure S2a shows the focal mechanism of the NESS1 events. Normal, strike-slip and thrust focal mechanisms are included, with a dominance of strike-slip events.

Figure S2b shows the average shear-wave velocity in the uppermost 30 m ($V_{S,30}$) assigned on the direct measurement of the S-waves velocity profile or inferred from empirical correlation with the topographic slope.

Ground motion parameters

Figure S3 shows that the D100 PGA and PGV residual distributions are roughly normally distributed with almost zero median and standard deviations equal to 0.65 and 0.59, respectively.

Figure S4 shows the FN, FP and vertical (V) cumulative distributions of PGA and SA at T = 0.1, 1.0 and 3.0s relative to the waveforms recorded over the fault surface projection (R_{JB} < 1 km)

[1]Francesca Pacor, Istituto Nazionale di Geofisica e Vulcanologia, Milan, Italy, francesca.pacor@ingv.it

CAPTIONS

Table S1. List of the 74 worldwide earthquake (sorted by time) collected in the NESS1 dataset: event-ID, data-time (UTC), event name, nation, moment magnitude (M_W), focal mechanism (FM), number of records (rec) and reference of fault geometry are reported.

Figure S1. Rupture distance R_{RUP} (a), line distance R_{LINE} (b) and nucleation point distance R_{NP} (c) versus Joyner and Boore distance R_{JB}.

Figure S2. Data-distribution in function of style of faulting: normal (*NF*), strike-slip (*SS*) and thrust fault (*TF*); and $V_{S,30}$ values according to measured S-waves velocity ($V_{S,30}$) profile (black) and surface geological information (white).

Figure S3. Histograms of the CB14 residuals for PGA and PGV of NESS1 dataset. Residuals Res are the difference between natural logarithms of observations and predictions. D100 values are used.

Figure S4. Cumulative distributions of different IMs (PGA, SA at 0.1, 1.0 and 3.0 s) observed at distances RJB $\leq$ 1 km for Fault-Parallel (FP, dotted line), Fault-Normal (FN, dashed line), and vertical (V, solid line) components. Number of data is also reported.

REFERENCE

Table S1

Ameri, G., A. Emolo, F. Pacor, and F. Gallovic (2011). Ground-Motion Simulations for the 1980 M 6.9 Earthquake (Southern Italy) and Scenario Events. Vol. 101, No. 3, pp. 1136-1151, doi: 10.1785/0120100231.

Ameri, G., F. Gallovic, and F. Pacor (2012). Complexity of the Mw 6.3 2009 L'Aquila (central Italy) earthquake: 2. Broadband strong motion modeling. J. Geophys. Res. 117, B04308

Ancheta, T.D., R.B. Darragh, J.P. Stewart, E. Seyhan, W.J. Silva, B.S.J. Chiou, K.E. Wooddell, R.W. Graves, A.R. Kottke, D.M. Boore, T. Kishida, and J.R. Donahue (2014). NGA-West2 Database. Earthq Spectra 30 (3): 989–1005.

Anderson, J.G., H. Kawase, G.P. Biasi, J.N. Brune, and S. Aoi (2013). Ground motions in the Fukushima Homadoru, Japan, normal-faulting earthquake. Bulletin of the Seismological Society of America 103(3): 1935-1951

Asano, K. and T. Iwata (2016). Source rupture processes of the foreshock and mainshock in the 2016 Kumamoto earthquake sequence estimated from the kinematic waveform inversion of strong motion data. Earth, Planets and Space, 68:147 DOI: 10.1186/s40623-016-0519-9

Asano, K. and T. Iwata (2006). Source process and near-source ground motions of the 2005 West Off Fukuoka Prefecture earthquake. Earth Planets Space, 58: 93–98.

Bernard, P., J.C. Gariel, and L. Dorbath (1997). Fault location and rupture kinematics of the magnitude 6.8, 1992 Erzincan earthquake, Turkey, from strong ground motion and regional records. Bull. Seism. Soc. Am., vol. 87(5): 1230-1243

Birgoren, G., H. Sekiguchi, and K. Irikura. 2004. Rupture model of the 1999 Duzce, Turkey, earthquake deduced from high and low frequency strong motion data. Geophys. Res. Lett.,Vol. 31, L05610, doi:10.1029/2003GL019194

Chiaraluce, L., R. Di Stefano, E. Tinti, L. Scognamiglio, M. Michele, E. Casarotti, M. Cattaneo, P. De Gori, C. Chiarabba, G. Monachesi, A. Lombardi, L. Valoroso, D. Latorre, and S. Marzorati (2017). The 2016 Central Italy Seismic Sequence: A First Look at the Mainshocks, Aftershocks, and Source Models. Seismological Society of America, Volume 88, Number 3. DOI: 10.1785/0220160221

Custodio, S., and R.J. Archuleta (2007). Parkfield earthquakes: Characteristic or complementary? Journal of Geophysical Research, vol. 112, B05310, doi:10.1029/2006JB004617.

Gallovic, F. (2016), Modeling velocity recordings of the Mw6.0 South Napa, California Earthquake: unilateral event with weak high-frequency directivity. Seismological Research Letters 87(1):2-14 · January 2016 DOI: 10.1785/0220150042

Gallovič, F., G. Ameri, J. Zahradník, J. Janský, V. Plicka, E. Sokos, A. Askan, and M. Pakzad (2013). Fault process and broadband ground-motion simulations of the 23 October 2011 Van (Eastern Turkey) earthquake, Bull. Seism. Soc. Am., 103, 3164-3178.

Hartzell, S., and C. Mendoza (1991). Application of an Iterative Least-Squares Wave-Form Inversion of Strong-Motion and Teleseismic Records to the 1978 Tabas, Iran, Earthquake. Bull. Seis. Soc. Am 81 (2):305-331

Hauksson, E., and S. Gross (1991). Source parameters of the 1933 Long Beach earthquake. Bull. Seism. Soc. Am., vol. 81, no. 1, pp. 81-98

Hernandez, B., M. Cocco, F. Cotton, S. Stramondo, O. Scotti, F. Courboulex, and M. Campillo (2004). Rupture history of the 1997 Umbria-Marche (central Italy) main shocks from the inversion of GPS, DInSAR and near field strong motion data. Annals of Geophysics 47 (4):1355-1376.

Hough, S.E., and D.S. Dreger (1995). Source parameters of the 23 April 1992 M 6.1 Joshua Tree, California, earthquake and its aftershocks: Empirical Green's function analysis of GEOS and TERRAscope data. Bull. Seism. Soc. Am., vol. 85, no. 6, pp. 1576-159

Oglesby, D.D., D.S. Dreger, R.A. Harris, N. Ratchkovski, and R. Hansen (2004). Inverse kinematic and forward dynamic models of the 2002 Denali fault earthquake, Alaska. Bull. Seis. Soc. Am. 94 (6):S214-S233.

Oppenheimer, D., J. Eaton, A. Jayko, M. Lisowski, G. Marshall, M. Murray, R. Simpson, R. Stein, G. Beroza, M. Magee, G. Carver, L. Dengler, R. McPherson, L. Gee, B. Romanowicz, F. Gonzalez, W.H. Li, K. Satake, P. Somerville, and D. Valentine (1993). The Cape Mendocino, California, earthquakes of April 1992: Subduction at the Triple Junction. Science, vol. 261, 23 July 1993, pp. 433-437

Paolucci, R., I. Mazzieri and C. Smerzini (2015). Anatomy of strong ground motion: near-source records and three-dimensional physics-based numerical simulations of the Mw 6.0 2012 May 29 Po Plain earthquake, Italy. Geophys. J. Int. (2015) 203, 2001–2020. doi: 10.1093/gji/ggv405

Pezzo, G., J.P. Merryman Boncori, C. Tolomei, S. Salvi, S. Atzori, A. Antonioli (2013). Coseismic Deformation and Source Modeling of the May 2012 Emilia (Northern Italy) Earthquakes. Seismological Research Letters 84(4):645-655. DOI: 10.1785/0220120171

Saltogianni, V., M. Gianniou, T. Taymaz, S. Yolsal-Çevikbilen, and S. Stiros (2015), Fault slip source models for the 2014 Mw 6.9 Samothraki-Gökçeada earthquake (North Aegean Trough) combining geodetic and seismological observations, J. Geophys. Res. Solid Earth, 120, 8610–8622, doi:10.1002/2015JB012052.

Talebian M., J. Biggs, M. Bolourchi, A. Copley, A. Ghassemi, M. Ghorashi, J. Hollingsworth, J. Jackson, E. Nissen, B. Oveisi, B. Parsons, K. Priestley, and A. Saiidi (2006). The Dahuiyeh (Zarand) earthquake of 2005 February 22 in central Iran: reactivation of an intra-mountain reverse fault, Geophysical Journal International, 164, 137-148.

Tatar, M., J. Jackson, D. Hatzfeld, and E. Bergman (2007). The 2004 May 28 Baladeh earthquake (Mw 6.2) in the Alborz, Iran: overthrusting the South Caspian Basin margin, partitioning of oblique convergence and the seismic hazard of Tehran, Geophysical Journal International, 170, 249-261

Tinti, E., L. Scognamiglio, A. Michelini,and M. Cocco (2016), Slip heterogeneity and directivity of the ML6.0, 2016,Amatrice earthquake estimated with rapid finite-fault inversion, Geophys. Res.Lett., 43, 10,745–10,752, doi:10.1002/2016GL071263.

Yagi, Y., and R. Okuwaki (2015), Integrated seismic source model of the 2015 Gorkha, Nepal, earthquake, Geophys. Res. Lett., 42, doi:10.1002/2015GL064995.

Yagi, Y., and M. Kikuchi (2000). Source rupture process of the Kocaeli, Turkey, earthquake of August 17, 1999, obtained by joint inversion of near-field data and teleseismic data. Geophys. Res. Lett. 27 (13):1969-1972.

Table S1. List of the 74 worldwide earthquake (sorted by time) collected in the NESS1 dataset: event-ID, data-time (UTC), event name, nation, moment magnitude (M_W), focal mechanism (FM), number of records (rec) and reference of fault geometry are reported.

#	Event-ID	Event data-time	Event name	Nation	M_W	FM	rec	reference
1	USA-1933-01554	1933-03-10 17:54:00	Long Beach	USA	6.4	SS	1	Hauksson and Gross, 1991
2	USGS-iscgem846894	1966-06-28 04:26:16	Parkfield	USA	6	SS	2	Custodio and Archuleta, 2007
3	USGS-iscgem787038	1971-02-09 14:00:40	San Fernando	USA	6.7	TF	27	Ancheta et al., 2014 (NGA-West2 database)
4	IT-1976-0002	1976-05-06 20:00:12	Friuli 1st shock	Italy	6.4	TF	1	DISS3.1.1 database
5	UZ-1976-0001	1976-05-17 02:58:41	Gazli	Uzbekistan	6.7	TF	1	Ambraseys et al., 2004
6	IT-1976-0027	1976-09-15 03:15:18	Friuli 2nd shock	Italy	5.9	TF	2	DISS3.1.1 database
7	IT-1976-0030	1976-09-15 09:21:18	Friuli 3rd shock	Italy	6	TF	5	DISS3.1.1 database
8	IT-1978-0004	1978-04-15 23:33:47	Patti Gulf	Italy	6	SS	2	DISS3.1.1 database
9	USGS-usp0000w1w	1978-08-13 22:54:51	Santa Barbara	USA	5.8	TF	5	Ancheta et al., 2014 (NGA-West2 database)
10	IR-1978-0002	1978-09-16 15:35:56	Tabas	Iran	7.3	TF	1	Hartzell, 1991 (SRCMOD database)
11	ME-1979-0003	1979-04-15 06:19:41	Montenegro 1st shosk	Montenegro	6.9	TF	5	Ambraseys et al., 2004
12	ME-1979-0012	1979-05-24 17:23:17	Montenegro 2nd shosk	Montenegro	6.2	TF	3	Ambraseys et al., 2004
13	USGS-usp000128g	1979-08-06 17:05:22	Coyote Lake	USA	5.8	SS	6	Ancheta et al., 2014 (NGA-West2 database)
14	USGS-usp00013ee	1979-10-15 23:16:57	Imperial Valley	Mexico	6.5	SS	27	Ancheta et al., 2014 (NGA-West2 database)
15	USGS-usp000181t	1980-06-09 03:28:19	Victoria	Mexico	6.3	SS	1	Ancheta et al., 2014 (NGA-West2 database)
16	IT-1980-0012	1980-11-23 18:34:53	Irpinia	Italy	6.9	NF	11	Ameri et al., 2011
17	USGS-usp0001dcq	1981-04-26 12:09:29	Westmorland	USA	5.9	SS	2	Ancheta et al., 2014 (NGA-West2 database)
18	IT-1984-0005	1984-05-11 10:41:48	Lazio-Abruzzo 2nd shock	Italy	5.5	NF	2	virtual fault
19	USGS-usp0002vtg	1986-07-08 09:20:43	North Palm Springs	USA	6.7	O	12	Ancheta et al., 2014 (NGA-West2 database)
20	GR-1986-0006	1986-09-13 17:24:34	Kalamata	Greece	5.9	NF	1	GreDaSS 2 database
21	USGS-usp0003afe	1987-11-24 13:15:56	Superstition Hills	USA	6.6	SS	2	Ancheta et al., 2014 (NGA-West2 database)
22	USGS-usp00040t8	1989-10-18 00:04:14	Loma Prieta	USA	6.9	TF	27	Ancheta et al., 2014 (NGA-West2 database)
23	TK-1992-0002	1992-03-13 17:18:39	Erzican	Turkey	6.6	SS	1	Bermard et al., 1997
24	USGS-usp000566s	1992-04-23 04:50:23	Joshua Tree	USA	6.1	SS	2	Hough and Dreger, 1995
25	USGS-usp00056e1	1992-04-25 18:06:04	Cape Mendocino 1st shock	USA	7	TF	7	Ancheta et al., 2014 (NGA-West2 database)
26	USGS-usp00056fp	1992-04-26 07:41:41	Cape Mendocino 2nd shock	USA	6.5	SS	2	Oppenheimer et al., 1993
27	USGS-usp00056g0	1992-04-26 11:18:26	Cape Mendocino 3rd shock	USA	6.7	SS	2	Oppenheimer et al., 1994
28	USGS-usp00059sn	1992-06-28 11:57:35	Landers	USA	7.3	SS	13	Cotton, 1995 (SRCMOD database)
29	GR-1993-0027	1993-07-14 12:31:48	Patras	Greece	5.6	SS	2	virtual fault
30	USGS-usp00066k9	1994-01-17 12:30:54	Northridge	USA	6.7	TF	44	Ancheta et al., 2014 (NGA-West2 database)
31	GR-1995-0017	1995-05-13 08:47:13	Kozani	Greece	6.6	NF	1	GreDaSS 2 database
32	GR-1995-0047	1995-06-15 00:15:47	Aigion	Greece	6.5	NF	2	virtual fault

33	TK-1995-0041	1995-10-01 15:57:12	Dinar	Turkey	6	NF	1	virtual fault
34	IT-1997-0004	1997-09-26 00:33:11	Umbria-Marche 1st shock	Italy	5.7	NF	1	Hernandez, 2004 (SRCMOD database)
35	IT-1997-0006	1997-09-26 09:40:24	Umbria-Marche 2nd shock	Italy	6	NF	3	DISS3.1.1 database
36	IT-1997-0137	1997-10-14 15:23:09	Umbria-Marche 3rd shock	Italy	5.6	NF	1	Hernandez, 2004 (SRCMOD database)
37	TK-1999-0077	1999-08-17 00:01:38	Kocaeli (Izmit) 1st shock	Turkey	7.6	SS	20	Yagi, 2000 (SRCMOD database)
38	TK-1999-0294	1999-09-13 11:55:27	Kocaeli (Izmit) 2nd shock	Turkey	5.8	SS	2	virtual fault
39	TK-1999-0415	1999-11-12 16:57:19	Duzce	Turkey	7.3	SS	14	Birgoren, 2004 (SRCMOD database)
40	JP-2000-0007	2000-10-06 04:30:17	Tottori	Japan	6.6	SS	8	Ancheta et al., 2014 (NGA-West2 database)
41	IR-2002-0035	2002-06-22 02:58:21	Changureh (Avaj)	Iran	6.4	TF	2	from aftershocks
42	USGS-usp000bg0m	2002-11-03 22:12:41	Denali	USA	7.86	SS	2	Oglesby, 2004 (SRCMOD database)
43	TK-2003-0038	2003-05-01 00:27:04	Bingöl	Turkey	6.33	SS	1	Ambraseys et al., 2004
44	IR-2003-0041	2003-12-26 01:56:53	Bam	Iran	6.5	SS	1	Ancheta et al., 2014 (NGA-West2 database)
45	IR-2004-0043	2004-05-28 12:38:43	Baladeh	Iran	6.4	TF	1	Tatar et al., 2007
46	USGS-nc51147892	2004-09-28 17:15:24	Parkfield	USA	5.98	SS	62	Ancheta et al., 2014 (NGA-West2 database)
47	JP-2004-0002	2004-10-23 08:55:58	Niigata 1st shock	Japan	6.6	TF	15	Ancheta et al., 2014 (NGA-West2 database)
48	JP-2004-0003	2004-10-27 01:40:49	Niigata 2nd shock	Japan	5.8	TF	1	virtual fault
49	JP-2004-0004	2004-12-14 05:56:10	Rumoi	Japan	5.7	TF	1	virtual fault
50	IR-2005-0044	2005-02-22 02:25:21	Dahuiyeh (Zarand)	Iran	6.5	TF	3	Talebian et al., 2006
51	JP-2005-0002	2005-03-20 01:53:41	Fukuoka Prefecture	Japan	6.6	SS	1	Asano, 2006 (SRCMOD database)
52	EMSC-20070716_0000038	2007-07-16 01:13:21	Chuetsu-oki	Japan	6.6	TF	2	Ancheta et al., 2014 (NGA-West2 database)
53	EMSC-20080613_0000091	2008-06-13 23:43:46	Iwate	Japan	6.9	TF	13	Ancheta et al., 2014 (NGA-West2 database)
54	IT-2009-0009	2009-04-06 01:32:40	L'Aquila	Italy	6.1	NF	5	Ameri, 2012
55	IT-2009-0102	2009-04-07 17:47:37	L'Aquila (aftershock)	Italy	5.5	NF	8	virtual fault
56	EMSC-20100903_0000044	2010-09-03 16:35:46	Darfield	New Zealand	7.1	SS	33	Ancheta et al., 2014 (NGA-West2 database)
57	EMSC-20110221_0000047	2011-02-21 23:51:42	Christchurch 1st shock	New Zealand	6.2	TF	14	Ancheta et al., 2014 (NGA-West2 database)
58	EMSC-20110222_0000004	2011-02-22 01:50:28	Christchurch 2nd shock	New Zealand	5.6	SS	3	virtual fault
59	EMSC-20110411_0000023	2011-04-11 08:16:12	Fukushima Homadoru	Japan	6.6	TF	12	Anderson, 2013
60	EMSC-20110613_0000006	2011-06-13 02:20:50	Christchurch 3rd shock	New Zealand	6	SS	9	virtual fault
61	EMSC-20111023_0000031	2011-10-23 10:41:22	Van	Turkey	7.3	TF	1	Gallovic et al., 2013
62	IT-2012-0008	2012-05-20 02:03:50	Emilia 1st shock	Italy	6.1	TF	1	Pezzo et al., 2013
63	IT-2012-0011	2012-05-29 07:00:02	Emilia 2nd shock	Italy	6	TF	24	Paolucci et al., 2015
64	IT-2012-0010	2012-05-29 10:55:56	Emilia aftershock	Italy	5.5	TF	7	virtual fault
65	IT-2012-0032	2012-05-29 11:00:22	Emilia aftershock	Italy	5.5	TF	8	virtual fault
66	EMSC-20140401_0000093	2014-04-01 23:46:48	Iquique	Chile	8.1	TF	8	virtual fault
67	EMSC-20140524_0000026	2014-05-24 09:25:01	Samothraki-Gökçeada	Greece	6.5	SS	2	Saltogianni et al., 2015

68	EMSC-20140824_0000036	2014-08-24 10:20:43	South Napa	USA	6.07	SS	13	Gallovic, 2016
69	EMSC-20150425_0000021	2015-04-25 06:11:26	Nepal	Nepal	7.8	TF	1	Yagi and Okuwaki, 2015 (SRCMOD database)
70	USGS-us20005iis	2016-04-15 16:25:06	Kumamoto-shi	Japan	7	NF	31	Asano et al., 2016
71	EMSC-20160824_0000006	2016-08-24 01:36:32	Amatrice	Italy	6	NF	7	Tinti, 2016
72	EMSC-20161026_0000095	2016-10-26 19:18:06	Ussita	Italy	5.9	NF	14	Chiaraluce et al., 2017
73	EMSC-20161030_0000029	2016-10-30 06:40:18	Norcia	Italy	6.5	NF	49	Chiaraluce et al., 2017
74	EMSC-20161113_0000048	2016-11-13 11:02:58	Kaikoura	New Zealand	8	SS	145	virtual fault

References

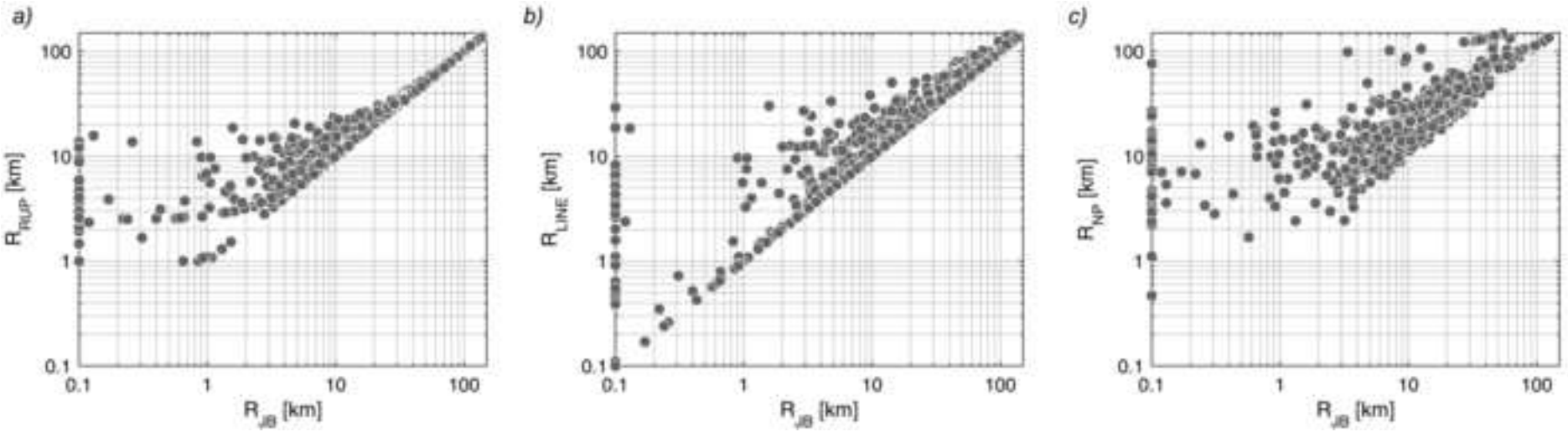

Supplemental Material (Figures)

Click here to download Supplemental Material (Main Page, Tables, and Figures)
Figure_S2.png

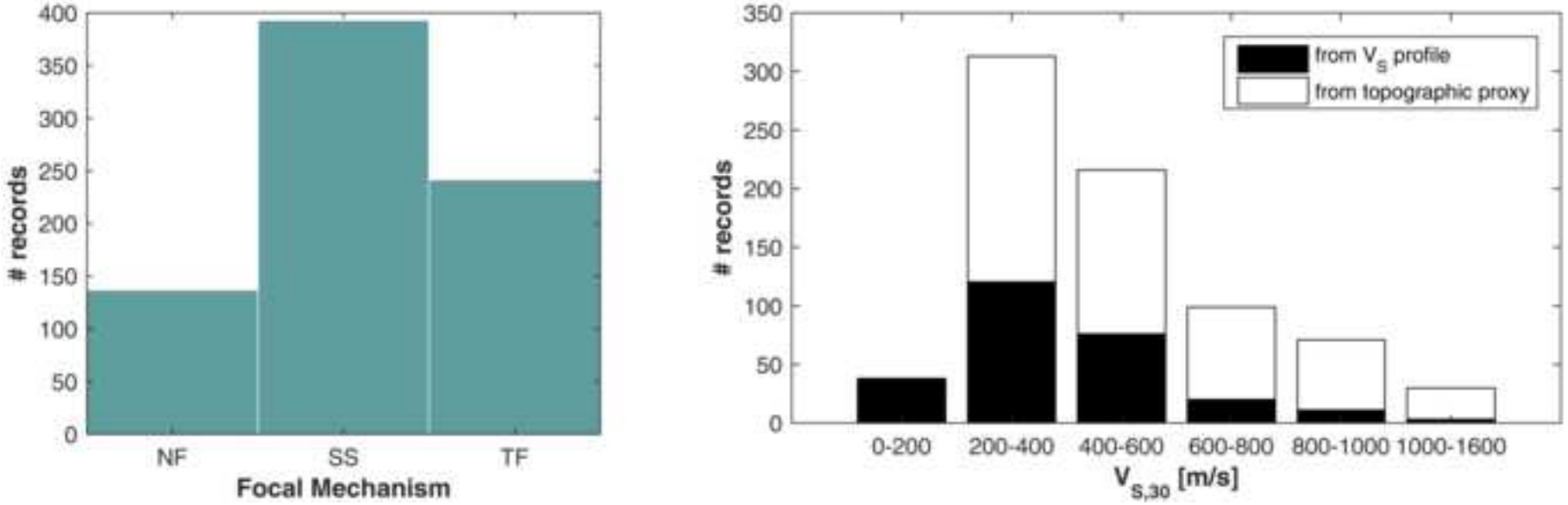

Supplemental Material (Figures)

Click here to download Supplemental Material (Main Page, Tables, and Figures)
Figure_S3.png

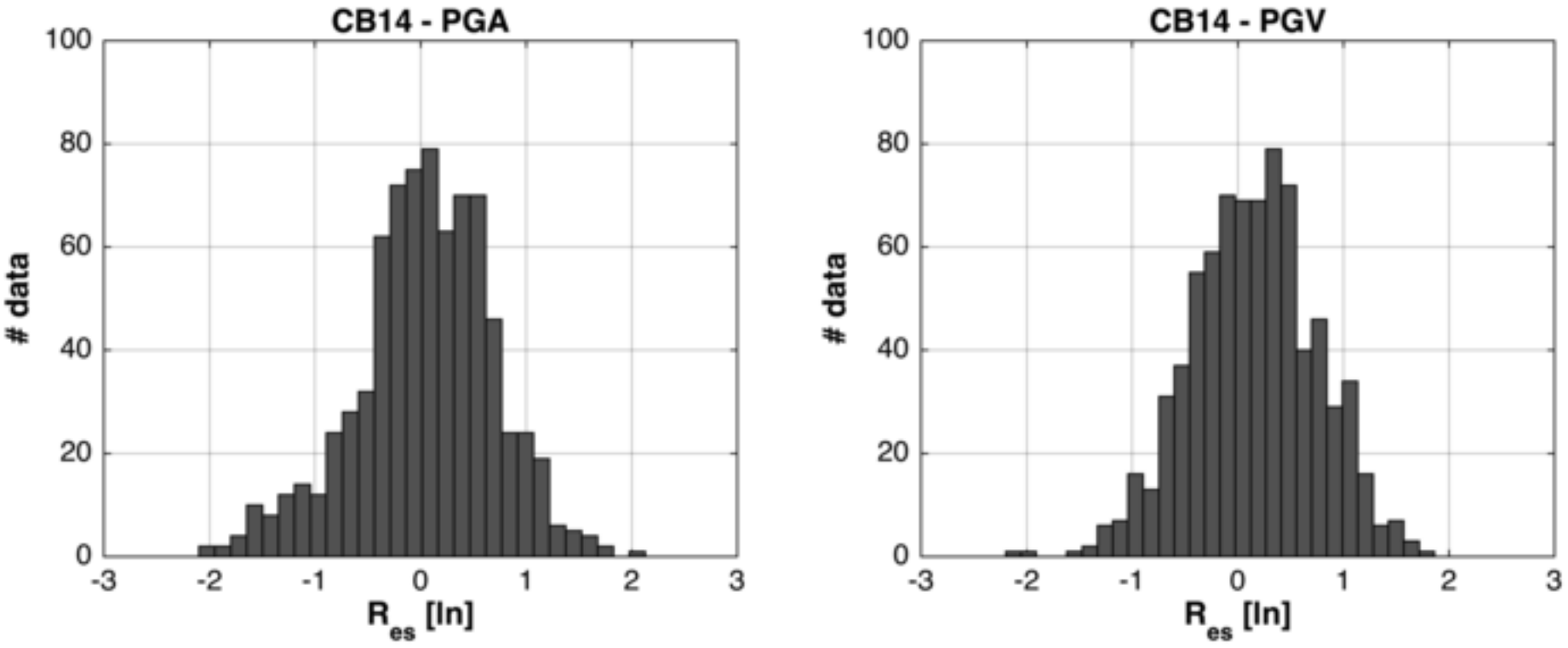

Click here to download Supplemental Material (Main Page, Tables, and Figures)
Figure_S4.png